# Manuscript Details

| | |
|---|---|
| **Manuscript number** | JCOMB_2018_4120 |
| **Title** | Isogeometric static and dynamic analysis of laminated and sandwich composite plates using nonpolynomial shear deformation theory |
| **Article type** | Full Length Article |


**Abstract**

An effective numerical approach based on the isogeometric analysis (IGA) employing nonpolynomial shear deformation theory (NPSDT) has been proposed and implemented in the present work for the static and dynamic analysis of laminated and sandwich composite plates. The theory assumes the nonlinear distribution of transverse shear stresses, and also satisfy the zero transverse shear deformation at the top and bottom surfaces of the laminates. Using Hamilton's principle, the governing equation of motion is derived and then discretized based on the IGA technique, which facilitates the use of non-uniform rational B-splines (NURBS) basis functions to easily satisfy the stringent continuity requirement of the NPSDT model (C 1-continuity) without any additional variables. The set of governing equations are solved to obtain transient response using Newmark's time integration scheme. Fourier transformation is carried out on the transient response to obtain the natural frequency. Various numerical examples covering different features of present modeling for laminated and sandwich plates are investigated. The performance of the model has been observed by comparing the evaluated results with different published results available in the open literature which ascertain its precision and range of applicability at a reduced computational cost.



| | |
|---|---|
| **Keywords** | Non-uniform rational B-splines (NURBS); Isogeometric analysis (IGA); Nonpolynomial shear deformation theory (NPSDT); Fast Fourier transform (FFT); Dynamic analysis; Composite plates. |
| **Manuscript region of origin** | Asia Pacific |



| | |
|---|---|
| **Corresponding Author** | Anup Ghosh |
| **Corresponding Author's Institution** | Indian Institute of Technology Kharagpur |
| **Order of Authors** | Anup Ghosh, Abha Gupta |
| **Suggested reviewers** | Hari Voruganti, Ann Jeffers, Sachin Singh Gautam, rajagopal amritham |


## Submission Files Included in this PDF

**File Name [File Type]**

1_CoverLetter__Manuscript_COMP_PartB_Dec_2018.pdf [Cover Letter]

Manuscript_COMP_PartB_Dec_2018.pdf [Manuscript File]

To view all the submission files, including those not included in the PDF, click on the manuscript title on your EVISE Homepage, then click 'Download zip file'.

December 10, 2018

To
Professor D. Hui
Editor-in-Chief
Journal of Composites Part B: Engineering

Dear Professor,

I would like to submit our manuscript entitled "Isogeometric static and dynamic analysis of laminated and sandwich composite plates using nonpolynomial shear deformation theory" for consideration as research article in Journal of Composites Part B: Engineering.

In this paper, an effective numerical approach based on the isogeometric analysis (IGA) employing nonpolynomial shear deformation theory (NPSDT) has been proposed and implemented for the static, free vibration and transient analysis of laminated and sandwich composite plates. Also, a Fourier transformation is performed on the transient response to obtain the natural frequency.

We have carried out an extensive comparative study of total computational time versus total number of elements and found that the IGA-NPSDT approach is more efficient and computationally faster than the FEA-NPSDT and results are relatively close to the analytical solution. This important aspect has a far reaching impact on the complex real world problem over FEM like aerospace, automotive etc., where large number of elements are required.

We do confirm that this work is original and has not been published elsewhere nor is it currently under consideration for publication elsewhere. All authors have approved the manuscript and agree with its submission to Journal of Composites Part B: Engineering.

We look forward to your editorial decision on this manuscript. Thank you for your time and consideration.

Your sincerely

Prof. Anup Ghosh
Assistant Professor,
Department of Aerospace Engineering
Indian Institute of Technology Kharagpur
West Bengal-721302, India
Phone No. +91-3222-283010
Email: anup@aero.iitkgp.ac.in

# Isogeometric static and dynamic analysis of laminated and sandwich composite plates using nonpolynomial shear deformation theory

Abha Gupta[1], Anup Ghosh[2,*]

*Department of Aerospace Engineering, Indian Institute of Technology Kharagpur, W. Bengal 721302, India*

**Abstract**

An effective numerical approach based on the isogeometric analysis (IGA) employing nonpolynomial shear deformation theory (NPSDT) has been proposed and implemented in the present work for the static and dynamic analysis of laminated and sandwich composite plates. The theory assumes the nonlinear distribution of transverse shear stresses, and also satisfy the zero transverse shear deformation at the top and bottom surfaces of the laminates. Using Hamilton's principle, the governing equation of motion is derived and then discretized based on the IGA technique, which facilitates the use of non-uniform rational B-splines (NURBS) basis functions to easily satisfy the stringent continuity requirement of the NPSDT model ($C^1$-continuity) without any additional variables. The set of governing equations are solved to obtain transient response using Newmark's time integration scheme. Fourier transformation is carried out on the transient response to obtain the natural frequency. Various numerical examples covering different features of present modeling for laminated and sandwich plates are investigated. The performance of the model has been observed by comparing the evaluated results with different published results available in the open literature which ascertain its precision and range of applicability at a reduced computational cost.

*Keywords:* Non-uniform rational B-splines (NURBS), Isogeometric analysis (IGA), Nonpolynomial shear deformation theory (NPSDT), Fast Fourier transform (FFT), Dynamic analysis, Composite plates

## 1. Introduction

Laminated and sandwich composites are widely used in aerospace, civil, mechanical, marine and other fields of modern technology due to their high strength-to-weight ratio, high stiffness-to-weight ratio, high impact, fatigue and corrosion resistance, etc. In addition to this, composite possess ability to tailor through optimization of ply numbers and fiber orientations so that they can meet the specific requirement while minimizing the weight [1]. These materials show prominent transverse shear effect due to their low shear to extensional rigidity, in comparison to the traditional material. Moreover, modeling of interlaminar shear stresses becomes more critical in the laminated plates and is more complex in sandwich structures. Therefore, the development of an appropriate model which is capable of accurately predicting the behavior of these laminated and sandwich structures is in great need.

Investigation on the properties of composite structures has been addressed for a long time [2, 3]. It is well known that an exact three-dimensional (3D) approach is the most potential tool to obtain the accurate solution for both thick and thin structures. However, it is not easy to solve practical problems in which complex geometric and boundary conditions are involved. Alternatively, several plate theories can be utilized as a reduction of the 3D full model to the two-dimensional (2D) model. In early stage of the development of structural models, the classical laminated plate theory (CLPT) [4] has been employed to predict the mechanical behavior of composite plates. However, CLPT ignores the effect of transverse shear deformation and hence become inappropriate for the analysis of thick plate. Later on first order shear deformation theory (FSDT), which includes constant transverse shear deformation with only $C^0$ continuity of generalized displacement became popular [5]. After that, a shear correction factor has been introduced to adjust the transverse shear energy. However, the dependency of the shear correction factor on the lamination sequence, loading conditions, and boundary conditions made it difficult to ascertain the accuracy of FSDT

*Corresponding author
*Email addresses:* abha.gupta91@gmail.com (Abha Gupta), anup@aero.iitkgp.ac.in (Anup Ghosh)
[1]Research Scholar
[2]Assistant Professor

[6]. Further, these limitations of FSDT have been overcome by the introduction of higher-order shear deformation theories (HSDTs). In general, transverse shear deformation are modeled using HSDT which either consider the displacement field of higher-order terms from Taylor's series expansion, called polynomial shear deformation theories (PSDTs) [7–9], or consider non-polynomial function in the displacement field, called non-polynomial shear deformation theory (NPSDT) [10–13]. Among various researchers, Reddy [9], Ambartsumian [14], Touratiour [15], Soldatos [16] have done noticeable work in the development of HSDT and detailed work on PSDT and NPSDT can be found in the review paper [17]. It is observed from the literature that the PSDTs give no significant improvement in the result after the third-order of polynomial series [18], whereas, NPSDT provides significantly large scope to increase the modeling accuracy.

It is well known that because of the limitations of analytical approach, various numerical methods have been developed such as FEM, BEM, smoothed FEM, mesh-free methods, etc. with its own advantages and disadvantages. Among different numerical techniques that seek approximate solutions, the finite element method (FEM) becomes a standard tool for the treatment of stress analysis problems. In FEM, the unknown field variables are approximated by linear combination of shape functions. Most existing finite elements and commercial codes use Lagrangian ($C^0$ inter-element continuity) and Hermitian ($C^1$ inter-element continuity) basis functions [19]. The Lagrangian shape functions, more commonly used in FEM, provide lower order approximation. And hence, the requirement of smooth geometry design and analysis with the demand of high precision and tighter integration paved the way for the development of new modeling-analysis process [20].

Ted Blacker from Sandia National Laboratory accounts that about 80% of overall analysis time is consumed for the modeling whereas 20% of overall time is actually devoted for the analysis [20]. This 80/20 ratio seems to be very common industrial experience and is, therefore, one of the major bottlenecks in computer-aided design (CAD)/ computer aided engineering (CAE)/ computer aided manufacturing (CAM) integration [21]. There is a great demand in industry for the integrated manufacturing process, design by means of CAD and analysis using CAE for the manufacturing done on CNC machines through

CAM. CAD and CAM industries rely on the use of NURBS based geometry [22, 23] for the shape representation; thus CAD/CAM integration is relatively straightforward. However, the use of different basis functions made the communication between CAD and CAE time-consuming, and hence there was a need to build a new finite element model which utilizes same basis function and at the same time maintain the compatibility with existing practices.

For the execution of analysis on geometric CAD model with higher order continuity, Hughes et al. in 2005 introduce a new technique named isogeometric analysis [20] to bridge the gap between CAD and FEA. Instead of Lagrange or Hermit basis functions, the isogeometric finite element method relies on NURBS basis functions, same as almost every CAD or CAM packages do. Based on the isoparametric concept, the NURBS basis function from the CAD technology is employed for both the parameterization of the geometry and the approximation of the plate deformation. Further, IGA has been applied to structural mechanics problem not only for the geometrical accuracy that it provides, but also for the high quality of stress fields resulting from the use of higher continuous basis functions. Several research papers have reported the use of isogeometric approach for the composite plate and shell analysis [24–26], linear and nonlinear elasticity and plasticity problem [27, 28]. Modeling using NURBS provide advantageous properties for structural vibrations problems [29–31] than higher-order FE p-methods. Based on IGA, few papers are available in the open literature in the field of static [32–35], free vibration [36–41], and transient analysis [42–45] of laminated and sandwich structure utilizing various polynomial and nonpolynomial shear deformation theories.

This paper proposes an effective numerical approach to investigate static and dynamic isogeometric analysis using inverse hyperbolic shear deformation theory (IHSDT) [46]. The Hamilton's principle is utilized to construct the weak form of the equation of the motion and solved using Newmark's integration scheme. Natural frequency of the composite plate has been obtained using the fast Fourier transform (FFT) of the transient time domain solution. IGA based MATLAB codes are developed to satisfy the $C^1$-continuity requirement in the discretization process using NURBS elements.The computational efficacy of the present approach has been measured. It is observed that recently proposed nonpolynomial shear

deformation theory [46] in conjunction with IGA is efficient for the analysis of the laminated and sandwich composite plates.

## 2. Nonpolynomial shear deformation theory for composite plates

A multilayered composite plate of dimension $a \times b \times h$, consist of $k$ orthotropic ply stacked in particular orientation is considered. A schematic diagram of laminated composite plate in the Cartesian coordinate system $(X - Y - Z)$ is shown in Fig. 1.

[Fig. 1 about here.]

### *2.1. Displacement field model*

For the nonpolynomial shear deformation theory, the plate deformation at any arbitrary point in the plate can be expressed in terms of field variables as

$$\begin{aligned} u(x,y,z) &= u_0(x,y) - z\frac{\partial w_0}{\partial x} + f(z)\,\theta_x(x,y) \\ v(x,y,z) &= v_0(x,y) - z\frac{\partial w_0}{\partial y} + f(z)\,\theta_y(x,y) \\ w(x,y,z) &= w_0(x,y) \end{aligned} \tag{1}$$

where $u_0$, $v_0$, and $w_0$ are the displacements along the mid-plane of the plate; $\theta_x$ and $\theta_y$ are the shear deformation at the mid-plane. The function $f(z) = (g(z) + z\Omega)$ incorporate the nonlinearity in transverse strain and represent the warping of the cross-section perpendicular to mid-plane. For the present study, an inverse hyperbolic shear deformation theory (IHSDT) [46] is employed by considering $g(z) = sinh^{-1}\left(\frac{rz}{h}\right)$ and $\Omega = -\frac{2r}{h}\frac{1}{\sqrt{r^2+4}}$ with $r = 3$ in which $h$ is the thickness of the plate.

### 2.2. Strain-displacement relation

The state-of-strain, $\boldsymbol{\epsilon}$ at a point corresponding to nonpolynomial displacement fields, in the Cartesian coordinate, is expressed as

$$\boldsymbol{\epsilon} = \begin{Bmatrix} \frac{\partial u}{\partial x} \\ \frac{\partial v}{\partial y} \\ \frac{\partial u}{\partial y} + \frac{\partial v}{\partial x} \\ \frac{\partial v}{\partial z} + \frac{\partial w}{\partial y} \\ \frac{\partial u}{\partial z} + \frac{\partial w}{\partial x} \end{Bmatrix} = \begin{bmatrix} \frac{\partial}{\partial x} & 0 & -z\frac{\partial^2}{\partial x^2} & f\left(z\right)\frac{\partial}{\partial x} & 0 \\ 0 & \frac{\partial}{\partial y} & -z\frac{\partial^2}{\partial y^2} & 0 & f\left(z\right)\frac{\partial}{\partial y} \\ \frac{\partial}{\partial y} & \frac{\partial}{\partial x} & -2z\frac{\partial^2}{\partial x \partial y} & f\left(z\right)\frac{\partial}{\partial y} & f\left(z\right)\frac{\partial}{\partial x} \\ 0 & 0 & 0 & 0 & f'(z) \\ 0 & 0 & 0 & f'(z) & 0 \end{bmatrix} \begin{Bmatrix} u_0 \\ v_0 \\ w_0 \\ \theta_x \\ \theta_y \end{Bmatrix} \tag{2}$$

The strain vector $\boldsymbol{\epsilon}$ followed from Eq. (1) can be written as summation of in-plane strain vector $\boldsymbol{\epsilon_p} = \left\{\epsilon_{xx}\ \epsilon_{yy}\ \gamma_{xy}\right\}^T = \boldsymbol{\epsilon_{p1}} + z\boldsymbol{\epsilon_{p2}} + g(z)\boldsymbol{\epsilon_{p3}}$ and transverse shear strain vector $\boldsymbol{\epsilon_s} = \left\{\gamma_{yz}\ \gamma_{xz}\right\}^T = \boldsymbol{\epsilon_{s1}} + g'\left(z\right)\boldsymbol{\epsilon_{s2}}$.

$$\boldsymbol{\epsilon} = \begin{Bmatrix} \boldsymbol{\epsilon_p} \\ \boldsymbol{\epsilon_s} \end{Bmatrix}, \quad \boldsymbol{\epsilon_p} = \begin{Bmatrix} \frac{\partial u}{\partial x} \\ \frac{\partial v}{\partial y} \\ \frac{\partial u}{\partial y} + \frac{\partial v}{\partial x} \end{Bmatrix}, \quad \boldsymbol{\epsilon_s} = \begin{Bmatrix} \frac{\partial v}{\partial z} + \frac{\partial w}{\partial y} \\ \frac{\partial u}{\partial z} + \frac{\partial w}{\partial x} \end{Bmatrix} \tag{3}$$

where,

$$\boldsymbol{\epsilon_p} = \begin{Bmatrix} \frac{\partial u_o}{\partial x} \\ \frac{\partial v_o}{\partial y} \\ \frac{\partial u_o}{\partial y} + \frac{\partial v_o}{\partial x} \end{Bmatrix} + z \begin{Bmatrix} -\frac{\partial^2 w_o}{\partial x^2} + \Omega\frac{\partial \theta_x}{\partial x} \\ -\frac{\partial^2 w_o}{\partial y^2} + \Omega\frac{\partial \theta_y}{\partial y} \\ -2\frac{\partial^2 w_o}{\partial x \partial y} + \Omega\left(\frac{\partial \theta_x}{\partial y} + \frac{\partial \theta_y}{\partial x}\right) \end{Bmatrix} + g(z) \begin{Bmatrix} \frac{\partial \theta_x}{\partial x} \\ \frac{\partial \theta_y}{\partial y} \\ \frac{\partial \theta_x}{\partial y} + \frac{\partial \theta_y}{\partial x} \end{Bmatrix} \tag{4}$$

$$\boldsymbol{\epsilon_s} = \Omega \begin{Bmatrix} \theta_y \\ \theta_x \end{Bmatrix} + \frac{\partial g}{\partial z} \begin{Bmatrix} \theta_y \\ \theta_x \end{Bmatrix}$$

In Eq. (4), the presence of second-order derivative operator requires $C^1$ continuity of field variable, specifically $w_0$. For Navier type analytical solution, $C^1$ continuity is easily achieved; however numerical method like FEM, which utilized Lagrange element, gives at most $C^0$ continuity of field variables. The reduction of $C^1$ to $C^0$ continuity requirement in FEM using Lagrange element is achieved by imposing an artificial constraint [47]. So,

after incorporating the constraint, the finite element model contains seven field variables. However, IGA can satisfy $C^1$ and higher order continuity because of the use of NURBS basis function in it; therefore it utilizes only five field variables [48], and as a result no artificial constraints are needed in the strain energy expression.

### *2.3. Constitutive equation*

The constitutive equation for an arbitrary $k^{th}$ orthotropic layer in global coordinate for plane stress problem is given by the Hooke's law as

$$\boldsymbol{\sigma}^{(k)} = \left[\mathcal{T}_{trans}^{(k)}\right] \boldsymbol{Q} \left[\mathcal{T}_{trans}^{(k)}\right]^T \boldsymbol{\epsilon}^{(k)} = \bar{\boldsymbol{Q}}^{(k)} \boldsymbol{\epsilon}^{(k)} \tag{5}$$

which may be elaborated as

$$\begin{Bmatrix} \sigma_{xx} \\ \sigma_{yy} \\ \sigma_{xy} \\ \sigma_{yz} \\ \sigma_{xz} \end{Bmatrix}^{(k)} = \left[\mathcal{T}_{trans}^{(k)}\right] \begin{bmatrix} Q_{11} & Q_{12} & Q_{16} & 0 & 0 \\ Q_{21} & Q_{22} & Q_{26} & 0 & 0 \\ Q_{61} & Q_{62} & Q_{66} & 0 & 0 \\ 0 & 0 & 0 & Q_{44} & Q_{45} \\ 0 & 0 & 0 & Q_{54} & Q_{55} \end{bmatrix} \left[\mathcal{T}_{trans}^{(k)}\right]^T \begin{Bmatrix} \epsilon_{xx} \\ \epsilon_{yy} \\ \gamma_{xy} \\ \gamma_{yz} \\ \gamma_{xz} \end{Bmatrix}^{(k)} \tag{6}$$

where, $\boldsymbol{\sigma}$, $\boldsymbol{\epsilon}$ and $\bar{\boldsymbol{Q}}$ are stress vector, strain vector, and the material constant matrix in the global coordinate, respectively. And $[\mathcal{T}_{trans}]$ is the local-to-global transformation matrix [49]. Due to symmetry in the orthotropic material $Q_{21} = Q_{12}$, $Q_{61} = Q_{16}$, $Q_{62} = Q_{26}$, and $Q_{54} = Q_{45}$; each material matrix coefficient can be expressed as

$$Q_{11} = \frac{E_1}{1 - \nu_{12}\nu_{21}},\ Q_{12} = \frac{\nu_{12}E_2}{1 - \nu_{12}\nu_{21}},\ Q_{22} = \frac{E_2}{1 - \nu_{12}\nu_{21}}$$

$$Q_{66} = G_{12},\ Q_{44} = G_{23},\ Q_{55} = G_{13}$$

Above, $E_1$ and $E_2$ are the Young's modulus; $G_{12}$, $G_{23}$, and $G_{13}$ are the shear modulus; and $\nu_{12}$ and $\nu_{21}$ are major and minor Poisson's ratios. Where, 1 represents longitudinal direction, and 2 and 3 represent transverse direction.

The in-plane forces, moments and shear forces are defined as

$$\left[\begin{array}{ccc} \boldsymbol{N} & \boldsymbol{M} & \boldsymbol{P} \end{array}\right] = \left[\begin{array}{ccc} N_{xx} & M_{xx} & P_{xx} \\ N_{yy} & M_{yy} & P_{yy} \\ N_{xy} & M_{xy} & P_{xy} \end{array}\right] = \int_{-h/2}^{h/2} \left\{\begin{array}{c} \sigma_{xx} \\ \sigma_{yy} \\ \sigma_{xy} \end{array}\right\} \left\{\begin{array}{ccc} 1 & z & g\left(z\right) \end{array}\right\} dz$$
$$\left[\begin{array}{cc} \boldsymbol{Q} & \boldsymbol{L} \end{array}\right] = \left[\begin{array}{cc} Q_{yz} & L_{yz} \\ Q_{xz} & L_{xz} \end{array}\right] = \int_{-h/2}^{h/2} \left\{\begin{array}{c} \sigma_{yz} \\ \sigma_{xz} \end{array}\right\} \left\{\begin{array}{cc} 1 & g'\left(z\right) \end{array}\right\} dz \tag{7}$$

Now, substituting Eq. (5) into Eq. (7), a generalized stress vector, $\hat{\boldsymbol{\sigma}}$ can be written in term of generalized strain vector, $\hat{\boldsymbol{\epsilon}}$ by following expression

$$\hat{\boldsymbol{\sigma}} = \left\{\begin{array}{c} \boldsymbol{N} \\ \boldsymbol{M} \\ \boldsymbol{P} \\ \boldsymbol{Q} \\ \boldsymbol{L} \end{array}\right\} = \left[\begin{array}{ccccc} \boldsymbol{A} & \boldsymbol{B} & \boldsymbol{E} & 0 & 0 \\ \boldsymbol{B} & \boldsymbol{D} & \boldsymbol{F} & 0 & 0 \\ \boldsymbol{E} & \boldsymbol{F} & \boldsymbol{H} & 0 & 0 \\ 0 & 0 & 0 & \boldsymbol{A}^s & \boldsymbol{B}^s \\ 0 & 0 & 0 & \boldsymbol{B}^s & \boldsymbol{D}^s \end{array}\right] \left\{\begin{array}{c} \boldsymbol{\epsilon_{p1}} \\ \boldsymbol{\epsilon_{p2}} \\ \boldsymbol{\epsilon_{p3}} \\ \boldsymbol{\epsilon_{s1}} \\ \boldsymbol{\epsilon_{s2}} \end{array}\right\} = \hat{\boldsymbol{D}}\,\hat{\boldsymbol{\epsilon}} \tag{8}$$

where

$$\left(\begin{array}{cccccc} \boldsymbol{A}_{ij} & \boldsymbol{B}_{ij} & \boldsymbol{D}_{ij} & \boldsymbol{E}_{ij} & \boldsymbol{F}_{ij} & \boldsymbol{H}_{ij} \end{array}\right) = \int_{-h/2}^{h/2} \left(\begin{array}{cccccc} 1 & z & z^2 & g(z) & zg(z) & g(z)^2 \end{array}\right) \bar{\boldsymbol{Q}}_{\boldsymbol{ij}}\, dz \qquad i,j = 1,2,6.$$

$$\left(\begin{array}{ccc} \boldsymbol{A}^{\boldsymbol{s}}_{\boldsymbol{ij}} & \boldsymbol{B}^{\boldsymbol{s}}_{\boldsymbol{ij}} & \boldsymbol{D}^{\boldsymbol{s}}_{\boldsymbol{ij}} \end{array}\right) = \int_{-h/2}^{h/2} \left(\begin{array}{ccc} 1 & g'(z) & g'(z)^2 \end{array}\right) \bar{\boldsymbol{Q}}_{\boldsymbol{ij}}\, dz \qquad i,j = 4,5$$

*2.4. Equations of motion*

For arbitrary space variable and admissible virtual displacement $\delta\left\{u\,,v\,,w\right\}$, Hamilton's principle of the given system is written as

$$\delta \int_{t_i}^{t_f} \mathcal{L} dt = \int_{t_i}^{t_f} \left(\delta\mathcal{K} - \delta\mathcal{U} + \delta\mathcal{W}_{ext}\right) dt = 0 \tag{9}$$

The first term in the Eq. (9) represents the virtual kinetic energy and is expressed as

$$\delta\mathcal{K} = -\int_V \rho\, \delta\boldsymbol{u}^T\, \ddot{\boldsymbol{u}}\, dz\, d\Omega \tag{10}$$

where $\rho$ is the mass density per unit volume, and $\boldsymbol{u}$ is the displacement vector. By following Eq. (1), displacement vector, $\boldsymbol{u}$ can be written in matrix form as

$$\boldsymbol{u} = \boldsymbol{Z}\,\bar{\boldsymbol{u}} \tag{11}$$

which may be elaborated as

$$\begin{Bmatrix} u \\ v \\ w \end{Bmatrix} = \begin{bmatrix} 1 & 0 & 0 & f(z) & 0 & -z & 0 \\ 0 & 1 & 0 & 0 & f(z) & 0 & -z \\ 0 & 0 & 1 & 0 & 0 & 0 & 0 \end{bmatrix} \begin{Bmatrix} u_0 \\ v_0 \\ w_0 \\ \theta_x \\ \theta_y \\ w_{0,x} \\ w_{0,y} \end{Bmatrix}$$

By substituting Eq. (11) in the Eq. (10) and integrating about Z-direction. The virtual kinetic energy can be rewritten as

$$\delta\mathcal{K} = -\int_{\Omega} \delta\bar{\boldsymbol{u}}^T \boldsymbol{m}\,\ddot{\bar{\boldsymbol{u}}}\,d\Omega \tag{12}$$

where $\boldsymbol{m}$ is the mass matrix, defined by

$$\boldsymbol{m} = \int_{-h/2}^{h/2} \rho\,\boldsymbol{Z}^T\,\boldsymbol{Z}\,dz$$

The second term in the Eq. (9) represents the virtual strain energy and is expressed in terms of generalized stress and strain vector as

$$\delta\mathcal{U} = \int_{\Omega} \delta\hat{\boldsymbol{\epsilon}}^T \hat{\boldsymbol{\sigma}}\,d\Omega = \int_{\Omega} \delta\hat{\boldsymbol{\epsilon}}^T\,\hat{\boldsymbol{D}}\,\hat{\boldsymbol{\epsilon}}\,d\Omega \tag{13}$$

The last term of the Eq. (9) is the virtual work done by transverse mechanical load and is expressed as

$$\delta\mathcal{W}_{ext} = \int_{\Omega} \delta w_0 P_w(x, y, t)\,d\Omega \tag{14}$$

where $P_w\,(x, y, t)$ is the distributed transverse load.

## 3. Isogeometric formulation for composite plate

### *3.1. NURBS functions and surfaces*

After decades of technology improvement, NURBS provides users with great control over the object shape in an intuitive way with low memory consumption making them the most widespread technique for geometry representation [22, 23]. In this subsection, various fundamental components related to B-spline and NURBS like knot vectors, rational or non-rational basis function are discussed.

#### *3.1.1. Knot vectors*

A parametric space is partitioned into elements by a knot vector, $\Xi$ in each direction, which is a non-decreasing set of coordinates in one-dimension [22, 23]. The knot vector is written as

$$\Xi = \{\xi_1, \xi_2, ....., \xi_j, ....., \xi_{n+p+1}\} \tag{15}$$

where the length of the knot vector is defined as, $|\Xi| = n + p + 1$. Here $\xi_j$ denotes the $j^{th}$ knot, $j$ is the knot index, $n$ is the number of basis functions and $p$ is the polynomial degree. In general, there are two main classes of knot vectors namely periodic and open, and the further classification depends on the arrangement of knot values [23].

Open knot vectors are standard in the CAD literature. In one-dimension, basis functions formed from open knot vectors are interpolatory at the ends of the parametric space interval, $[\xi_1, \xi_{n+p+1}]$, but are not interpolatory at the interior knots. This feature makes knots, in isogeometric analysis, different from nodes, in finite element analysis (FEA). An open non-uniform knot vector can be conducive to attain much richer behavior in the characteristics of basis functions used in IGA [50].

#### *3.1.2. Basis functions*

Given a knot vector, the B-spline basis functions, $N^b_{i,p}(\xi)$ of degree, $p = 0$ are defined as

$$N_{i,0}^{b}(\xi) = \begin{cases} 1, & \xi_i \leq \xi < \xi_{i+1} \\ 0, & \text{otherwise} \end{cases}$$

The basis functions of degree $p > 0$ are defined by the following Cox-de Boor recursion formula [22].

$$N_{i,p}^{b}(\xi) = \frac{\xi - \xi_i}{\xi_{i+p} - \xi_i} N_{i,p-1}^{b}(\xi) + \frac{\xi_{i+p+1} - \xi}{\xi_{i+p+1} - \xi_{i+1}} N_{i+1,p-1}^{b}(\xi) \tag{16}$$

Which means that basis functions are in parametric form in contrast to FEA, i.e., the Lagrange polynomials are explicit functions. Fig. 2 illustrates a set of one-dimensional quadratic, cubic, and quartic B-spline basis functions for open uniform knot vectors. A B-spline basis function is $C^{p-1}$ continuous at a single knot. A knot value can appear more than once and is then called a multiple knot. At a knot of multiplicity $\hat{k}$, the continuity is reduced to $C^{p-\hat{k}}$.

[Fig. 2 about here.]

*3.1.3. NURBS surface*

B-spline curves are defined as

$$C(\xi) = \sum_{i=1}^{n} N_{i,p}^{b}(\xi)\, P_i \tag{17}$$

where $P_i$ are the control points and $N_{i,p}^{b}(\xi)$ is the $p^{th}$-degree B-spline basis function defined on the open knot vector.

B-spline surfaces are defined by the tensor product of B-spline curves in two parametric dimensions $\xi$ and $\eta$ with two knot vectors, $\Xi = \{\xi_1, \xi_2, \ldots, \xi_{n+p+1}\}$ and $\mathcal{H} = \{\eta_1, \eta_2, \ldots, \eta_{m+q+1}\}$ and which is expressed as

$$S(\xi, \eta) = \sum_{i=1}^{n} \sum_{j=1}^{m} N_{i,p}^{b}(\xi) M_{j,q}^{b}(\eta) P_{i,j} \tag{18}$$

where $P_{i,j}$ is the bidirectional control net and $N^b_{i,p}(\xi)$ and $M^b_{j,q}(\eta)$ are the B-spline basis functions defined on the knot vectors $\Xi$ and $\mathcal{H}$ respectively, over an $n \times m$ net of control points, $P_{i,j}$.

The logical coordinate $(i,\ j)$ of B-spline surface is identically denoted as node "A" in context of FEM [25, 27] and Eq. (18) can be rewritten as

$$S(\xi,\eta) = \sum_{A=1}^{n\times m} N^b_A(\xi,\eta) P_A \tag{19}$$

where $N^b_A(\xi,\eta) = N^b_{i,p}(\xi)\, M^b_{j,q}(\eta)$ is the shape function associated with a control point $A$. The superscript $b$ indicates that $N^b_A$ is a B-spline shape function.

NURBS curves and surfaces are the generalization of B-splines curves and surfaces. A NURBS entity in $\mathbb{R}^d$ Euclidean space is obtained by projecting a B-spline entity in $\mathbb{R}^{d+1}$, where d is the number of physical dimensions. NURBS basis functions are obtained by augmenting every control point, $P_A$, in control mesh with the homogeneous coordinate $w_A$, which are scalar in nature, also known as weights. Given weights to the control points, make NURBS curves/surfaces rational, which are additional parameters demonstrating the projection from projective geometry. The weighting function is constructed as follow:

$$w^g(\xi,\eta) = \sum_{A=1}^{n\times m} N^b_A(\xi,\eta)\, w_A \tag{20}$$

where $w^g(\xi,\eta)$ is the common denominator function. The NURBS surfaces are then defined by

$$S(\xi,\eta) = \frac{\sum_{A=1}^{n\times m} N^b_A(\xi,\eta) w_A P_A}{w^g(\xi,\eta)} = \sum_{A=1}^{n\times m} R_A(\xi,\eta)\, P_A \tag{21}$$

where $R_A(\xi,\eta) = N^b_A(\xi,\eta) w_A / w^g(\xi,\eta)$ is the NURBS basis function.

The choice of the weight in the NURBS basis function depends on the CAD model considered for the analysis and which can be calculated [22, 23] using Eq. (21). For rectangular geometry, B-spline basis functions are sufficient to represent the geometry accurately by considering $w^g_A = 1$ [22, 23], which is a special case of NURBS basis functions.

The B-spline (or NURBS) can be enriched by three types of refinements - knot insertion, degree elevation (or order elevation), and degree and continuity elevation. The first two are equivalent to h- and p-refinement, respectively, while the last one is k-refinement that does not exist in standard FEM [20].

### *3.2. NURBS based discretization*

Using NURBS basis functions, we interpolate the displacement fields of the plate which can be written as

$$\boldsymbol{u} = \begin{Bmatrix} u_0 \\ v_0 \\ w_0 \\ \theta_x \\ \theta_y \end{Bmatrix} = \sum_{I=1}^{(p+1)\times(q+1)} \begin{bmatrix} R_I & 0 & 0 & 0 & 0 \\ 0 & R_I & 0 & 0 & 0 \\ 0 & 0 & R_I & 0 & 0 \\ 0 & 0 & 0 & R_I & 0 \\ 0 & 0 & 0 & 0 & R_I \end{bmatrix} \begin{Bmatrix} u_{0I} \\ v_{0I} \\ w_{0I} \\ \theta_{xI} \\ \theta_{yI} \end{Bmatrix} \tag{22}$$

where $(p+1)\times(q+1)$ is the number of basis functions and $R_I\,(\xi,\eta)$ and $\mathbf{q}_I = \{u_{0I}\ v_{0I}\ w_{0I}\ \theta_{xI}\ \theta_{yI}\}^T$ are the NURBS basis functions and the degrees of freedom associated with control point $I$, respectively.

Substituting Eq. (22) into Eq. (3), the generalized strain vector, $\hat{\boldsymbol{\epsilon}}$ can be rewritten in terms of elemental displacement vector, $\boldsymbol{q}$ and elemental strain-displacement matrix, $\boldsymbol{B}^L$, having degree, $(p,\, q) = 2$

$$\hat{\boldsymbol{\epsilon}} = \sum_{I=1}^{9} \boldsymbol{B}_I^L\, \boldsymbol{q}_I = \boldsymbol{B}^L\, \boldsymbol{q} \tag{23}$$

in which

$$\boldsymbol{B}_I^L = \begin{bmatrix} \left(\boldsymbol{B}_I^{p1}\right)^T & \left(\boldsymbol{B}_I^{p2}\right)^T & \left(\boldsymbol{B}_I^{p3}\right)^T & \left(\boldsymbol{B}_I^{s1}\right)^T & \left(\boldsymbol{B}_I^{s2}\right)^T \end{bmatrix}^T$$

$$\boldsymbol{q} = \begin{Bmatrix} u_{01} & v_{01} & w_{01} & \theta_{x1} & \theta_{y1} & \cdots & u_{09} & v_{09} & w_{09} & \theta_{x9} & \theta_{y9} \end{Bmatrix}^T$$

where $\boldsymbol{B}_I$ is a strain-displacement matrix written in terms of NURBS basis function and its derivatives.

$$\boldsymbol{B}_I^{p1} = \begin{bmatrix} R_{I,x} & 0 & 0 & 0 & 0 \\ 0 & R_{I,y} & 0 & 0 & 0 \\ R_{I,y} & R_{I,x} & 0 & 0 & 0 \end{bmatrix} \qquad \boldsymbol{B}_I^{p2} = \begin{bmatrix} 0 & 0 & -R_{I,xx} & \Omega R_{I,x} & 0 \\ 0 & 0 & -R_{I,yy} & 0 & \Omega R_{I,y} \\ 0 & 0 & -2R_{I,xy} & \Omega R_{I,y} & \Omega R_{I,x} \end{bmatrix}$$

$$\boldsymbol{B}_I^{p3} = \begin{bmatrix} 0 & 0 & 0 & R_{I,x} & 0 \\ 0 & 0 & 0 & 0 & R_{I,y} \\ 0 & 0 & 0 & R_{I,y} & R_{I,x} \end{bmatrix} \qquad \boldsymbol{B}_I^{s1} = \begin{bmatrix} 0 & 0 & 0 & 0 & \Omega R_I \\ 0 & 0 & 0 & \Omega R_I & 0 \end{bmatrix}$$

$$\boldsymbol{B}_I^{s2} = \begin{bmatrix} 0 & 0 & 0 & 0 & R_I \\ 0 & 0 & 0 & R_I & 0 \end{bmatrix}$$

The first and second derivatives of NURBS basis functions, used in strain-displacement matrix, can be calculated in terms of B-spline basis functions [20] as shown below:

$$\frac{\partial R_i(\xi,\eta)}{\partial \xi} = w_i \left( \frac{1}{w^g} \frac{\partial N_i^b(\xi,\eta)}{\partial \xi} - \frac{w^g_{,\xi}}{(w^g)^2} N_i^b(\xi,\eta) \right)$$

$$\frac{\partial^2 R_i(\xi,\eta)}{\partial \xi^2} = w_i \left( \frac{1}{w^g} \frac{\partial^2 N_i^b(\xi,\eta)}{\partial \xi^2} - 2\frac{w^g_{,\xi}}{(w^g)^2} \frac{\partial N_i^b(\xi,\eta)}{\partial \xi} - \frac{w^g_{,\xi\xi}}{(w^g)^2} N_i^b(\xi,\eta) + 2\frac{\left(w^g_{,\xi}\right)^2}{(w^g)^3} N_i^b(\xi,\eta) \right)$$

$$\frac{\partial^2 R_i(\xi,\eta)}{\partial \xi \partial \eta} = w_i \left( \frac{1}{w^g} \frac{\partial^2 N_i^b(\xi,\eta)}{\partial \xi \partial \eta} - \frac{w^g_{,\xi}}{(w^g)^2} \frac{\partial N(\xi,\eta)}{\partial \eta} - \frac{w^g_{,\eta}}{(w^g)^2} \frac{\partial N(\xi,\eta)}{\partial \xi} - \frac{w^g_{,\xi\eta}}{(w^g)^2} N_i^b(\xi,\eta) + 2\frac{w^g_{,\xi} w^g_{,\eta}}{(w^g)^3} N_i^b(\xi,\eta) \right) \tag{24}$$

where,

$$w^g = \sum_{j=1}^{n} w_j N_j^b(\xi,\eta) \qquad w^g_{,\xi} = \sum_{j=1}^{n} w_j \frac{\partial N_j^b(\xi,\eta)}{\partial \xi}$$

$$w^g_{,\xi\xi} = \sum_{j=1}^{n} w_j \frac{\partial^2 N_j^b(\xi,\eta)}{\partial \xi^2} \qquad w^g_{,\xi\eta} = \sum_{j=1}^{n} w_j \frac{\partial^2 N_j^b(\xi,\eta)}{\partial \xi \partial \eta}$$

To calculate the derivatives of NURBS in Eq. (24), $k^{th}$ derivative of B-spline basis function is required and the same can be obtained by following formula [20]

$$\frac{d^k}{d\xi^k} N^b_{i,p}(\xi) = \frac{p!}{(p-k)!} \sum_{j=0}^{k} \beta_{k,j} N^b_{i+j,p-k}(\xi)$$

$$\begin{aligned}
\beta_{0,0} &= 1 && k = 0,\ j = 0 \\
\beta_{k,0} &= \frac{\beta_{k-1,j}}{\xi_{i+p+j-k+1} - \xi_{i+j}} && j = 0 \\
\beta_{k,k} &= \frac{-\beta_{k-1,j-1}}{\xi_{i+p+j-k+1} - \xi_{i+j}} && j = k \\
\beta_{k,j} &= \frac{\beta_{k-1,j} - \beta_{k-1,j-1}}{\xi_{i+p+j-k+1} - \xi_{i+j}} && j = 1, \cdots, k-1
\end{aligned}$$

Using Eqs. (12)–(14), (22) and (23) in Eq. (9), and eliminating the virtual displacement vector, $\delta \boldsymbol{q}$, the system of equations of motion for transient analysis (or initial value problem) [51] can be obtained in following matrix form

$$\boldsymbol{K}\boldsymbol{q} + \boldsymbol{M}\ddot{\boldsymbol{q}} = \boldsymbol{F_m} \tag{25}$$

where $\boldsymbol{K}$, $\boldsymbol{M}$ and $\boldsymbol{F_m}$ are the stiffness, mass matrix and force vector, respectively.

***Stiffness matrix.***

$$\boldsymbol{K} = \int \boldsymbol{B^L}^T \hat{\boldsymbol{D}}\, \boldsymbol{B^L} d\Omega$$

***Mass matrix.***

$$\boldsymbol{M} = \int_\Omega [\mathcal{R}]^T\, \boldsymbol{m}\, [\mathcal{R}]\, d\Omega$$

Also,

$$[\mathcal{R}]\, \boldsymbol{q} = \sum_{I=1}^{9} [\mathcal{R}_I]\, \boldsymbol{q_I}$$

where

$$[\mathcal{R}_I] = \begin{bmatrix} R_I & 0 & 0 & 0 & 0 \\ 0 & R_I & 0 & 0 & 0 \\ 0 & 0 & R_I & 0 & 0 \\ 0 & 0 & 0 & R_I & 0 \\ 0 & 0 & 0 & 0 & R_I \\ 0 & 0 & R_{I,x} & 0 & 0 \\ 0 & 0 & R_{I,y} & 0 & 0 \end{bmatrix}$$

***Force vector***.

$$\boldsymbol{F_m} = \int_{\Omega} \{\mathcal{W}\}^T P_w\,(x, y, t)\, d\Omega$$

Also,

$$\{\mathcal{W}\}\,\boldsymbol{q} = \sum_{I=1}^{9} \{\mathcal{W}_I\}\,\boldsymbol{q_I}$$

where

$$\{\mathcal{W}_I\} = \left\{ \begin{array}{ccccc} 0 & 0 & R_I & 0 & 0 \end{array} \right\}$$

By neglecting the effect of external force in Eq. (25), the governing set of equations for free vibration analysis (or eigenvalue problem) [49] is obtained as

$$\boldsymbol{M\ddot{q}} + \boldsymbol{Kq} = 0$$

Similarly, the system of equilibrium equations for static analysis (or boundary value problem) [49] is obtained by neglecting the influence of inertial force from Eq. (25) as

$$\boldsymbol{Kq} = \boldsymbol{F}_m$$

## 4. Numerical results

In this section, numerical results of static and dynamic analyses of laminated and sandwich composite plates using NURBS based isogeometric approach in conjunction with NPSDT are presented.

### *4.1. Material properties*

Following sets of material properties are used in this section:

- Material-I: [49]

  $E_1/E_2 = 25, \quad G_{12}/E_2 = 0.5, \quad G_{13}/E_2 = 0.5, \quad G_{23}/E_2 = 0.2, \quad \nu_{12} = 0.25.$

- Material-II: [52]

$$Q_{core} = \begin{bmatrix} 0.999781 & 0.231192 & 0 & 0 & 0 \\ 0.231192 & 0.524886 & 0 & 0 & 0 \\ 0 & 0 & 0.262931 & 0 & 0 \\ 0 & 0 & 0 & 0.266810 & 0 \\ 0 & 0 & 0 & 0 & 0.159914 \end{bmatrix}$$

$$Q_{facesheet} = \mathcal{R} \times Q_{core}; \qquad \text{where} \quad \rho_{facesheet} = \mathcal{R} \times \rho_{core}$$

- Material-III: [53]

  Face sheets:

  $E_1 = 276\ GPa, \quad E_2 = G_{12} = G_{13} = G_{23} = 6.9\ GPa, \quad \nu_{12} = 0.25, \quad \rho = 681.8\ kg/m^3.$

  Core:

  $E_1 = E_2 = 0.5776\ GPa, \quad G_{12} = G_{13} = 0.1079\ GPa, \quad G_{23} = 0.22215\ GPa, \quad \nu_{12} = 0.0025, \quad \rho = 1000\ kg/m^3.$

- Material-IV: [54]

  $E_1 = 276\ GPa, \quad E_2 = 6.9\ GPa, \quad G_{12} = G_{13} = 4.14\ GPa, \quad G_{23} = 3.45\ GPa, \quad \nu_{12} = 0.25, \quad \rho = 1578\ kg/m^3.$

- Material-V: [55]

  $E_1 = 525\ GPa, \quad E_2 = 21\ GPa, \quad G_{12} = G_{23} = G_{13} = 10.5\ GPa, \quad \nu_{12} = 0.25, \quad \rho = 800\ kg/m^3.$

- Material-VI: [43]

  $E_1 = 172.369\ GPa, \quad E_2 = 6.895\ GPa, \quad G_{12} = G_{13} = 3.448\ GPa, \quad G_{23} = 1.379\ GPa, \quad \nu_{12} = 0.25, \quad \rho = 1603.03\ kg/m^3.$

- Material-VII: [56]

  $E_1 = 30 \times 10^6\ psi, \quad E_2 = 0.75 \times 10^6\ psi, \quad G_{12} = 0.45 \times 10^6\ psi, \quad G_{23} = G_{13} = 0.37 \times 10^6\ psi, \quad \nu_{12} = 0.25, \quad \rho = 0.000143\ lb\, sec^2/in^4.$

- Material-VIII: [54]

$E_1 = 181\ GPa,\quad E_2 = 10.3\ GPa,\quad G_{12} = G_{13} = 7.17\ GPa,\quad G_{23} = 2.87\ GPa,\quad \nu_{12} = 0.28,\quad \rho = 1578\ kg/m^3.$

- Material-IX: [57]

  $E_2 = 10^6\ psi,\quad E_1 = 40E_2,\quad G_{12} = G_{13} = 0.6E_2,\quad G_{23} = 0.5E_2,\quad \nu_{12} = 0.25,\quad \rho = 0.00012\ lb\,sec^2/in^4.$

### *4.2. Various dynamic loads*

The dynamic analysis of laminated and sandwich composite plates under different kinds of time dependent blast pulse load [58] is studied numerically by changing various parameters. The several form of blast loads are explained here.

- Step Loading

  For step loading, the expression for the load function can be written as

$$F(t) = \left\{ \begin{array}{ll} 1, & 0 \le t \le t_1 \\ 0, & t \ge t_1 \end{array} \right\} \tag{26}$$

- Sinusoidal Loading

  The sinusoidal pulse can be expressed mathematically as

$$F(t) = \left\{ \begin{array}{c} sin(\pi t/t_1),\quad 0 \le t \le t_1) \\ 0,\quad t \ge t_1 \end{array} \right\} \tag{27}$$

- Explosive Blast Loading

  If the explosion occurs at a far distant from the plate, then the blast pressure can be expressed as in terms of the Friedlander exponential decay equations as [59]

$$F(t) = \left\{ \begin{array}{ll} e^{-\Upsilon t}, & 0 \le t \le t_1 \\ 0, & t \ge t_1 \end{array} \right\} \tag{28}$$

  where, $\Upsilon$ denotes a decay parameter.

- Triangular Loading

  Sonic boom effect could be modeled as a N-shaped pressure pulse, and such a pulse corresponds to an idealized far-field overpressure produced by any supersonic flying object. The overpressure signature of the N-wave shock pulse can be described by

$$F(t) = \left\{ \begin{array}{l} 1 - t/t_1, \;\; 0 \leq t \leq rt_1 \\ 0, \;\; t \leq 0 \;\text{ and }\; t \geq rt_1 \end{array} \right\} \tag{29}$$

  where $r$ denotes the shock pulse length factor. The shape of the pulse depends on $r$. Note that: (i) for $r = 1$, N-shaped pulse degenerate into a triangular pulse or triangular blast refers to just a positive impulse; (ii) for $r = 2$ a symmetric N-shaped pressure pulse is obtained; while (iii) for $r > 2$ the N-shaped pulse becomes an asymmetric impulse.

*4.3. Boundary conditions*

As the present formulation is based on the displacement approach, so it is required to satisfy the kinematics boundary conditions ($u_0$, $v_0$, $w_0$, $\theta_x$, $\theta_y$) only. The different types of boundary conditions, most commonly occurring in practice are considered for isogeometric analysis of laminated and sandwich composite plate to assess the efficacy of the present approach.

- Simply supported

  1. For cross-ply

     SSSS-1 : $v_0 = w_0 = \theta_y = 0$ at $x = 0, a$ and $u_0 = w_0 = \theta_x = 0$ at $y = 0, b$.

  2. For angle-ply

     SSSS-2 : $u_0 = w_0 = \theta_y = 0$ at $x = 0, a$ and $v_0 = w_0 = \theta_x = 0$ at $y = 0, b$.

- Clamped

  1. CCCC : $u_0 = v_0 = w_0 = \theta_x = \theta_y = w_{0,x} = w_{0,y} = 0$ at $x = 0, a$ and $y = 0, b$.

### *4.4. Numerical examples and discussions*

Present subsection deals with some numerical investigations using NURBS based elements on static, free vibration and transient analysis of composite plates that includes validation and comparison of the present results with the analytical results as well as with the available numerical results. The obtained natural frequency from FFT analysis are validated with the present and available eigenvalue solution. Also, the computational efficacy of isogeometric approach is assessed in reference to the standard finite element approach.

In IGA, each knot span is the physical element, where actual integration is carried out. Also, each control point is associated with the NURBS basis function which makes them shared within the knot spans (elements). A $8 \times 8$ mesh of quadratic NURBS element is used for the present study or otherwise stated. Gauss-Legendre quadrature rule of integration has been employed in all the analysis with selective integration scheme as in FEM [60–62] to avoid shear locking behavior. The order of Gauss points $(p+1) \times (q+1)$ for bending, and $p \times q$ for transverse shear part have been used. Where $p$ and $q$ are the polynomial degrees of the NURBS basis functions in $X$ and $Y$ directions, respectively. The integration is carried out at each element, and the assembly is done at the control points, as IGA uses isoparametric mapping.

The discretization detail of the rectangular plate using mesh-size of $5 \times 5$ quadratic NURBS elements is shown in Fig. 3. It has been assumed that the thickness and the material for all the layers are the same, otherwise stated.

[Fig. 3 about here.]

**Static analysis**

This sub-subsection belongs to the description and discussion of various numerical solved examples for establishing the accuracy, efficiency, and applicability of the proposed isogeometric model using IHSDT for bending analysis. The continuous least square projection (CL2P) procedure [63] has been extended from FEA to IGA for stress recovery procedure [64]. The main idea of using CL2P as a stress recovery technique in IGA are: (i) local

extrapolation cannot be performed using basis function used in IGA because interior knots are not interpolatory, hence stresses are achieved on surfaces/contours itself, (ii) alternative to control points, to store the stress contour over whole domain at Gauss points requires a large amount of data space, which can be reduced by getting the stress values at the control point directly, (iii) by directly evaluating the gradient of field variables at the domain there is oscillation in the secondary variables like stresses and the same can be overcome, (iv) stresses now can be treated as a primary variable like displacement and hence accurate representation of stresses are achieved. Hence for the evaluation of stresses in IGA at control points with higher accuracy, CL2P stress recovery technique is used to obtain efficient results.

*4.4.1. Four-layered simply supported square laminated plate*

A sinusoidal transverse load is considered for the symmetric cross-ply square $(0^0/90^0/90^0/0^0)$ laminated plate. The plate is composed of four orthotropic layers $(Material - I)$ of equal thickness and is subjected to simply supported boundary condition. The numerical results for the nondimensional deflection and stresses for various span-to-thickness ratios, $a/h$ are obtained at critical points and are shown in Table 1. The results for deflection and stresses are enumerated with the following nondimensional forms as given below

$$\bar{w} = w_0 \left(\frac{a}{2}, \quad \frac{b}{2}\right) \left(\frac{100 E_2 h^3}{b^4 P_w}\right);$$

$$[\bar{\sigma}_{xx} \;\; \bar{\sigma}_{yy} \;\; \bar{\sigma}_{xy}] = [\sigma_{xx} \;\; \sigma_{yy} \;\; \sigma_{xy}] \left(\frac{h^2}{b^2 P_w}\right);$$

$$[\bar{\sigma}_{yz} \;\; \bar{\sigma}_{xz}] = [\sigma_{yz} \;\; \sigma_{xz}] \left(\frac{h}{b P_w}\right);$$

The present formulation is verified with the available results based on various shear deformation theories from the literature [9, 11, 46, 65, 66]. The accuracy of the present result with respect to closed-form solution may be well appreciated (see Table 1). Also, the through-thickness distribution of transverse shear stress based on present IGA model using

an inverse hyperbolic distribution is compared with other polynomial based model [46, 49]. It is clear from Fig. 4 that the present IGA-IHSDT formulation predicts the transverse shear stresses accurately and can be used to model the laminated plates efficiently.

[Fig. 4 about here.]

[Table 1 about here.]

*4.4.2. Three-layered simply supported square sandwich plate*

A simply supported square sandwich plate ($0^0/C/0^0$) with equal thickness ($h_f = 0.1h$) face sheets as shown in Fig. 5 with orthotropic core composed of material model given in $Material - II$ is analyzed under the effect of uniform load.

[Fig. 5 about here.]

The material properties of the face sheets are obtained by multiplying core properties by a parameter $\mathcal{R}$. Flexural response of a moderately thick plate is investigated for $\mathcal{R} = 5$ and 15. Transverse deflection and stresses are obtained at the critical points and the results are presented in the nondimensional forms as given below

$$\bar{w} = \frac{0.999781}{hP_w}\left(\frac{a}{2},\ \frac{b}{2},\ 0\right); \qquad \bar{\sigma}^1_{xx} = \frac{\sigma^1_{xx}}{P_w}\left(\frac{a}{2},\ \frac{b}{2},\ -\frac{h}{2}\right);$$

$$\bar{\sigma}^2_{xx} = \frac{\sigma^1_{xx}}{P_w}\left(\frac{a}{2},\ \frac{b}{2},\ -\frac{2h}{5}\right); \qquad \bar{\sigma}^3_{xx} = \frac{\sigma^2_{xx}}{P_w}\left(\frac{a}{2},\ \frac{b}{2},\ -\frac{2h}{5}\right);$$

$$\bar{\sigma}^1_{yy} = \frac{\sigma^1_{yy}}{P_w}\left(\frac{a}{2},\ \frac{b}{2},\ -\frac{h}{2}\right); \qquad \bar{\sigma}^2_{yy} = \frac{\sigma^1_{yy}}{P_w}\left(\frac{a}{2},\ \frac{b}{2},\ -\frac{2h}{5}\right);$$

$$\bar{\sigma}^3_{yy} = \frac{\sigma^2_{yy}}{P_w}\left(\frac{a}{2},\ \frac{b}{2},\ -\frac{2h}{5}\right);$$

In the above expression, superscript over the stresses, i.e., $\sigma_{ii}$ denotes the layer number of the sandwich plate. Numerical results obtained from the present IGA-IHSDT analysis are

validated with the existing numerical results based on different shear deformation theories [11, 46, 47, 67, 68] and with the closed-form solution (CFS) [52]. The results are presented in Table 2. It is observed that IGA results using IHSDT are not only in excellent agreement with the existing results but IGA-IHSDT results are more close to closed-form results than FEM-IHSDT results because of $C^1$-continuity.

[Table 2 about here.]

**Free Vibration analysis**

Numerous examples are solved to ensure the validity and accuracy of IGA-IHSDT solution for the prediction of eigenvalue. Fundamental natural frequency is obtained and the comparison is made with the existing results.

*4.4.3. Five-layered simply supported square sandwich plate*

A five-layered simply supported sandwich plate with symmetric face sheets $(0^0/90^0/C/90^0/0^0)$ is considered for the analysis. The material properties of core and face sheets are taken from $Material - III$. The ratio of core thickness to the total thickness $h_c/h$ is considered as 0.8 and the plies of face sheets are assumed to be of same thickness. The effect of the various span-to-thickness ratios, $a/h$ (6.67, 10, 20) on the nondimensional frequency parameter is observed using IGA-IHSDT and compared with the available solutions as shown in Table 3. The present theory is capable of predicting free vibration behavior of sandwich plates accurately. The results obtained using IGA-IHSDT formulation for sandwich plate are found to be closer to the analytical results [53] as compared with the other available results. Thus the present formulation has been validated for the free vibration analysis.

[Table 3 about here.]

#### *4.4.4. Higher modes of vibration for simply supported anti-symmetric cross-ply laminated plate*

In order to verify the accuracy for the prediction of higher vibration modes which is used in modal decomposition analysis, a study is conducted on anti-symmetric cross-ply laminated plate. A four-layered $(0^0/90^0/0^0/90^0)$ square laminated plate with span-to-thickness ratio, $a/h = 10$ is considered. Material properties used for the analysis is $Material - IV$ for each cross-ply with all edges simply supported. Nondimensional frequencies for first six modes are obtained using present IGA-IHSDT; and a closed form solution (CFS) is also obtained for comparison using method prescribed in the literature [53]. A comparison of present results with those available in literature are shown in Table 4. It is observed from the table that the present IGA-IHSDT formulation is also capable of accurately predicting the higher vibration mode of a system and results are in well agreement to closed-form solution.

[Table 4 about here.]

### Transient analysis

Time-dependent transient equations are solved using the unconditionally stable Newmark time integration scheme [51]. The values of $\alpha$ and $\beta$ are taken to be 0.5 and 0.25 (constant-average acceleration method) respectively or otherwise stated.

#### *4.4.5. Simply supported orthotropic plate under uniform step loading*

In order to validate the present technique, an orthotropic simply supported plate under uniformly distributed transverse load has been considered. The square plate with length, $a = 0.25\,m$ is analyzed using $Material - V$ for the span-to-thickness ratio, $a/h = 50$.

An uniform step loading of $1MPa$ is applied and response is taken at every time step of $\Delta t = 10^{-5}\,sec$ for $t_1 = 2 \times 10^{-3}\,sec$ as followed in the reference [55]. A transient response of a nondimensionalized central deflection, $\bar{w} = w/h$ is shown in Fig. 6. It is observed that the results obtained from IGA-IHSDT are in well match with the available finite strip method (FSM) by Chen et. al [55] and IGA-TSDT by Tran et. al [43]. Thus the present formulation has been validated accurately.

[Fig. 6 about here.]

Also, to assess the computational efficacy, the variation of total computational time with respect to total number of elements for both FEA and IGA is studied as shown in Fig. 7. The comparative study reveals that the IGA requires less computation power than FEA. As the total number of elements increases, the total simulation time of FEA increases drastically, whereas IGA computational time grows gradually, because for the same mesh size IGA requires less control points/ DOFs than FEA and hence IGA solution time is highly reduced. This important aspect of IGA has a far reaching impact on the complex real world problem over FEM where large number of elements are required.

[Fig. 7 about here.]

*4.4.6. Effect of various dynamic loadings on symmetric cross-ply laminated plate*

The dynamic response of three-layered $(0^0/90^0/0^0)$ thick plate is investigated using $Material-VI$ for the simply supported boundary condition. Sinusoidally distributed transverse load of magnitude 0.689 $GPa$ is used for the analysis of laminated plate with $a/h = 5$ and $h = 0.1526\ m$. Different time dependent impulse loadings: step, triangular, sinusoidal and explosive blast loading are considered for the analysis and results are shown in Fig. 8.

The response of nondimensionalized central deflection, $\bar{w} = w/h$ is taken at every time step of $\Delta t = 10^{-5} sec$ for $t_1 = 6 \times 10^{-3} sec$. The decay parameter, $\Upsilon$ considered in explosive blast loading is 660 $sec^{-1}$ as followed in the reference [43]. Fig. 8 shows the comparison of present results with the available result in the literature [43], which are found to be in good agreement.

[Fig. 8 about here.]

*4.4.7. Three-layered square sandwich plate under step loading*

A simply supported square sandwich plate with core thickness, $0.8h$ and face thickness $0.1h$ under sinusoidal and uniform transverse load is considered. The material properties

of the sandwich core and skin are given in $Material - II$, where $\rho_{core} = 1$. The skins material properties are related with the core properties by $\mathcal{R} = 15$. Isogeometric square sandwich composite plates with span-to-thickness ratio, $a/h = 10$ subjected to step loading is considered. For this case of sandwich plate, time step for Newmark's direct integration method [69] is $\Delta t = 10^{-2} sec$ where the values of $\alpha$ and $\beta$ are taken to be 3/2 and 8/5 with total simulation time, $t_1 = 25\, sec$ [69].

The plotting of central deflection, $w$ with time $t$ is shown in Fig. 9. It has been observed that the IGA-IHSDT results are in good agreement with the available analytical [69] and FEM-TSDT [69] results.

[Fig. 9 about here.]

*4.4.8. Nine-layered square laminated plate under N-shaped pressure pulse*

The dynamic response of nine-layered $(0^0/90^0/0^0)_3$ laminated plate is investigated using $Material - VII$. Uniformly distributed transverse load of magnitude $200\, psi$ is used for the analysis with $a/h = 20$ and $h = 3\ in$. The present analysis consider a symmetric and asymmetric N-shaped pressure pulse with $r = 2$ and 2.5 for $t_1 = 0.01\, sec$ and $0.004\, sec$ respectively as given in the literature [56]. Fig. 10 displays the time-history response of dimensionless central deflection ( $\bar{w} = w/h$) obtained for various pulse loads characterized by different $r$ and $t_1$ parameters. It can be seen from the Fig. 10 that the present IGA-IHSDT results are in well agreement with the HSDT results [56]. Hence, it may be concluded that the present IGA-IHSDT formulation is efficient for the transient analysis.

[Fig. 10 about here.]

*4.4.9. Time-history response and its Fourier transform for the square laminated plate*

A four-layered $(0^0/90^0/90^0/0^0)$ simply supported symmetric cross-ply square laminated plate is considered to determine the nondimensional natural frequency. Each cross-ply consist of orthotropic material, $Material - VIII$, with equal thickness. The effect of the

span-to-thickness ratio, $a/h$ on the nondimensional frequency using eigenvalue analysis is observed using IGA-IHSDT and compared with the available closed-form [46, 54] as well as 3-dimensional solutions [54]. A comparison of the present result for different $a/h$ (5, 10, 20) ratios is shown in Table 5. It is clear from the table that the eigenvalue solution using present IGA-IHSDT give results closer to the available closed-form solution [46].

Also, natural frequency has been calculated from transient response using fast Fourier transform (FFT) under step loading with spatial sinusoidal distributed load. In addition, Table 5 also shows that the natural frequency obtained using Fourier transformation is matching well with the natural frequency obtained from eigenvalue solution. The time-history response of dimensionless central deflection, $\bar{w} = w(100E_2h^3/P_wa^4)$ using IGA-IHSDT for $t_1 = 5\times10^{-3}sec$ and $\Delta t = 1\times10^{-6}sec$ and its Fourier transform has been shown in Fig. 11.

[Table 5 about here.]

[Fig. 11 about here.]

*4.4.10. Effect of various parameter on transient response of laminated composite plate*

In this sub-subsection, the effect of various parameters such as span-to-thickness ratio, $E_1/E_2$ ratio, fiber orientation, number of layers etc. have been studied on transient response of laminated composite plate. A parametric study utilizing IGA-IHSDT formulation is carried out, and new results are presented. The material property given in $Material - IX$ is used for the subsequent analysis. The geometric properties [57] of the problems below are $h = 2\,inch$, $a = b = 10h$. A sinusoidal loading for $t_1 = 0.003\,sec$ is applied with spatial sinusoidal distributed load [57] having magnitude, $P_w = 5\times10^3\,psi$ under clamped boundary condition. The time step, $\Delta t = 10^{-5}\,sec$ has been used in the following analysis.

The transient response of four-layered $(0^0/90^0/90^0/0^0)$ cross-ply laminated composite plate is investigated against the various span-to-thickness ratios, $(a/h = 5,\ 10,\ 15,\ \text{and}\ 20)$ and has been shown in the Fig. 12. It is observed in the figure that as span-to-thickness

ratio increases the central deflection of laminated plate also increases. This is due to the fact that thin laminated plate is more susceptible to the load effect than the thick one.

[Fig. 12 about here.]

The transient response of four-layered $(0^0/90^0/90^0/0^0)$ cross-ply laminated composite plate is analyzed for the various $E_1/E_2$ ratios ($E_1/E_2$ = 10, 20, 30, and 40) and has been shown in the Fig. 13. It has been observed that as $E_1/E_2$ ratio increases the magnitude of deflection decreases. This behavior of the plot may be explained as, the increase of $E_1/E_2$ ratio increases the stiffness of the plate. The plot also shows the free vibration response after the stated applied load for time duration of $t_1 = 0.003\, sec$.

[Fig. 13 about here.]

In the same way, the effect of number of layers on the transient response of angle-ply $(45^0/-45^0)_k$ laminated composite has been analyzed. The number of layer, $k$ = 1, 2, 3 and 4 have been considered for the analysis. The transient response is shown in the Fig. 14. It has been observed from the figure that as the number of layers increases, the deflection of the plate decreases and become indifferent for any significant change after $N = 4$ layer.

[Fig. 14 about here.]

Furthermore, the effect of fiber orientation on the transient response of angle-ply $(\theta/-\theta/\theta/-\theta)$ laminated composite plate has also been studied. The transient response for different fiber orientation ($\theta = 0^0$, $15^0$, $30^0$, and $45^0$) has been shown in the Fig. 15. It is observed from the figure that as the orientation angle increases the plate deflection decreases and the minimum response is obtained at $\theta = 45^0$.

[Fig. 15 about here.]

## 5. Conclusion

A flexible and efficient NURBS based solution for the inverse hyperbolic shear deformation theory (IHSDT) has been proposed. Due to higher inter element continuity of the NURBS basis functions, isogeometric formulation incorporating IHSDT requires five field variables unlike FEM $C^0$ formulation which needs seven field variables and hence the isogeometric analysis (IGA) reduces the order of the stiffness matrix. The effects of the various span-to-thickness ratio, $E_1/E_2$ ratio, and lamination sequence are observed for static, free vibration and transient analysis of the laminated plates and sandwich structures. The fast Fourier transform (FFT) analysis has been carried out to obtain natural frequency from the transient response. In case of structural vibration, frequency analysis plays an important role, as it makes designer aware about the natural frequency. The present FFT analysis is able to accurately predict the natural frequency as obtained from eigenvalue solution.

A comparative study of total computational time versus total number of elements shows that the IGA approach is more efficient and computationally faster. As total number of elements increases, the total simulation time for the IGA is far less than the FEA. Also for the same mesh size, IGA requires less field variables and control points due to higher inter-element continuity of the basis functions hence leads to reduced total degrees of freedom. Less DOFs means less memory consumption and less memory storage, consequently, cheaper in terms of DOFs. Hence, these features make IGA an efficient analysis framework for structural analysis.

It is observed that the IGA-IHSDT results are excellent for the prediction of the static and dynamic analysis of the laminated composite and sandwich plates. Also, IGA-IHSDT results are relatively close to the analytical solution in comparison to the finite element solutions for the same mesh size due to higher continuity. The results presented for the static and dynamic analysis of laminated and sandwich composite plate using IGA-IHSDT may be used as a benchmark solution for the nonpolynomial shear deformation theory (NPSDT). As no results have been reported in the literature using the present methodology and therefore the gap is rightly filled with the standard solution to provide a reference for the further

analysis using other NPSDT. It may be concluded that IGA methodology using IHSDT may be appreciated well for its efficient approach and better viability over FEM for static and dynamic analysis with reduced computational efforts.

## References


[1] Nikbakt S, Kamarian S, Shakeri M. A review on optimization of composite structures part i: Laminated composites. Composite Structures 2018;195:158–85.

[2] Whitney J, Pagano N. Shear deformation in heterogeneous anisotropic plates. Journal of applied mechanics 1970;37(4):1031–6.

[3] Vinson JR. The behavior of sandwich structures of isotropic and composite materials. Lancaster PA: Technomic Publishing Company; 1999.

[4] Timoshenko SP, Woinowsky-Krieger S. Theory of plates and shells. McGraw-hill; 1959.

[5] Reissner E. The effect of transverse shear deformation on the bending of elastic plates. Journal of Applied Mechanics 1945;:A69–77.

[6] Pai PF. A new look at shear correction factors and warping functions of anisotropic laminates. International Journal of Solids and Structures 1995;32(16):2295–313.

[7] Levinson M. An accurate, simple theory of the statics and dynamics of elastic plates. Mechanics Research Communications 1980;7(6):343–50.

[8] Lo K, Christensen R, Wu E. A high-order theory of plate deformation—part 2: Laminated plates. Journal of applied mechanics 1977;44(4):669–76.

[9] Reddy JN. A simple higher-order theory for laminated composite plates. Journal of applied mechanics 1984;51(4):745–52.

[10] Mantari J, Oktem A, Soares CG. Static and dynamic analysis of laminated composite and sandwich plates and shells by using a new higher-order shear deformation theory. Composite structures 2011;94(1):37–49.

[11] Mantari J, Oktem A, Soares CG. A new trigonometric shear deformation theory for isotropic, laminated composite and sandwich plates. International Journal of Solids and Structures 2012;49(1):43–53.

[12] Mantari J, Oktem A, Soares CG. A new higher order shear deformation theory for sandwich and composite laminated plates. Composites Part B: Engineering 2012;43(3):1489–99.

[13] El Meiche N, Tounsi A, Ziane N, Mechab I, et al. A new hyperbolic shear deformation theory for buckling and vibration of functionally graded sandwich plate. International Journal of Mechanical Sciences 2011;53(4):237–47.

[14] Ambartsumian S. On the theory of bending plates. Izv Otd Tech Nauk AN SSSR 1958;5(5):69–77.

[15] Touratier M. An efficient standard plate theory. International journal of engineering science 1991;29(8):901–16.

[16] Soldatos K. A transverse shear deformation theory for homogeneous monoclinic plates. Acta Mechanica 1992;94(3):195–220.

[17] Abrate S, Di Sciuva M. Equivalent single layer theories for composite and sandwich structures: A review. Composite Structures 2017;179:482–94.

[18] Ghugal Y, Shimpi R. A review of refined shear deformation theories of isotropic and anisotropic laminated plates. Journal of Reinforced Plastics and Composites 2002;21(9):775–813.

[19] Bhavikatti SS. Finite element analysis. New Age International, New Delhi; 2005.

[20] Hughes TJ, Cottrell JA, Bazilevs Y. Isogeometric analysis: Cad, finite elements, nurbs, exact geometry and mesh refinement. Computer methods in applied mechanics and engineering 2005;194(39):4135–95.

[21] Cottrell JA, Hughes TJ, Bazilevs Y. Isogeometric analysis: toward integration of CAD and FEA. New York, USA: John Wiley & Sons; 2009.

[22] Piegl L, Tiller W. The NURBS book (Monographs in Visual Communication). Second ed.; New York, USA: Springer-Verlag; 1997.

[23] Rogers D. An Introduction to NURBS: With Historical Perspective. San Diego, CA: Academic Press; 2001.

[24] Kiendl J, Bletzinger KU, Linhard J, Wüchner R. Isogeometric shell analysis with kirchhoff–love elements. Computer Methods in Applied Mechanics and Engineering 2009;198(49):3902–14.

[25] Benson D, Bazilevs Y, Hsu MC, Hughes T. Isogeometric shell analysis: the reissner–mindlin shell. Computer Methods in Applied Mechanics and Engineering 2010;199(5):276–89.

[26] Casanova CF, Gallego A. Nurbs-based analysis of higher-order composite shells. Composite Structures 2013;104:125–33.

[27] Thai CH, Nguyen-Xuan H, Nguyen-Thanh N, Le TH, Nguyen-Thoi T, Rabczuk T. Static, free vibration, and buckling analysis of laminated composite reissner–mindlin plates using nurbs-based isogeometric approach. International Journal for Numerical Methods in Engineering 2012;91(6):571–603.

[28] Liu N, Jeffers AE. Adaptive isogeometric analysis in structural frames using a layer-based discretization to model spread of plasticity. Computers & Structures 2018;196:1–11.

[29] Cottrell JA, Reali A, Bazilevs Y, Hughes TJ. Isogeometric analysis of structural vibrations. Computer methods in applied mechanics and engineering 2006;195(41):5257–96.

[30] Wang D, Liu W, Zhang H. Novel higher order mass matrices for isogeometric structural vibration analysis. Computer Methods in Applied Mechanics and Engineering 2013;260:92–108.

[31] Kiani Y. Isogeometric large amplitude free vibration of graphene reinforced laminated plates in thermal environment using nurbs formulation. Computer Methods in Applied Mechanics and Engineering

2018;332:86–101.

[32] Pavan G, Rao KN. Bending analysis of laminated composite plates using isogeometric collocation method. Composite Structures 2017;176:715–28.

[33] Liu N, Jeffers AE. Isogeometric analysis of laminated composite and functionally graded sandwich plates based on a layerwise displacement theory. Composite Structures 2017;176:143–53.

[34] Thai S, Thai HT, Vo TP, Nguyen-Xuan H. Nonlinear static and transient isogeometric analysis of functionally graded microplates based on the modified strain gradient theory. Engineering Structures 2017;153:598–612.

[35] Dufour JE, Antolin P, Sangalli G, Auricchio F, Reali A. A cost-effective isogeometric approach for composite plates based on a stress recovery procedure. Composites Part B: Engineering 2018;138:12 –8.

[36] Shojaee S, Valizadeh N, Izadpanah E, Bui T, Vu TV. Free vibration and buckling analysis of laminated composite plates using the nurbs-based isogeometric finite element method. Composite Structures 2012;94(5):1677–93.

[37] Peković O, Stupar S, Simonović A, Svorcan J, Trivković S. Free vibration and buckling analysis of higher order laminated composite plates using the isogeometric approach. Journal of Theoretical and Applied Mechanics 2015;53(2):453–66.

[38] Thai CH, Ferreira A, Bordas SPA, Rabczuk T, Nguyen-Xuan H. Isogeometric analysis of laminated composite and sandwich plates using a new inverse trigonometric shear deformation theory. European Journal of Mechanics-A/Solids 2014;43:89–108.

[39] Fantuzzi N, Tornabene F. Strong formulation isogeometric analysis (sfiga) for laminated composite arbitrarily shaped plates. Composites Part B: Engineering 2016;96:173 – 203.

[40] Shi P, Dong C, Sun F, Liu W, Hu Q. A new higher order shear deformation theory for static, vibration and buckling responses of laminated plates with the isogeometric analysis. Composite Structures 2018;204:342–58.

[41] Faroughi S, Shafei E, Eriksson A. Nurbs-based modeling of laminated composite beams with isogeometric displacement-only theory. Composites Part B: Engineering 2019;162:89 – 102.

[42] Kapoor H, Kapania R. Geometrically nonlinear nurbs isogeometric finite element analysis of laminated composite plates. Composite Structures 2012;94(12):3434–47.

[43] Tran LV, Lee J, Nguyen-Van H, Nguyen-Xuan H, Wahab MA. Geometrically nonlinear isogeometric analysis of laminated composite plates based on higher-order shear deformation theory. International Journal of Non-Linear Mechanics 2015;72:42–52.

[44] Phung-Van P, Ferreira A, Nguyen-Xuan H, Wahab MA. An isogeometric approach for size-dependent geometrically nonlinear transient analysis of functionally graded nanoplates. Composites Part B: En-

gineering 2017;118:125–34.

[45] Gupta A, Ghosh A. Transient analysis of anti-symmetric cross-ply and angle-ply laminated composite plates using nurbs-based isogeometric analysis. In: 58th AIAA/ASCE/AHS/ASC Structures, Structural Dynamics, and Materials Conference. 2017, p. 1980.

[46] Grover N, Maiti D, Singh B. A new inverse hyperbolic shear deformation theory for static and buckling analysis of laminated composite and sandwich plates. Composite Structures 2013;95:667–75.

[47] Grover N, Maiti D, Singh B. An efficient c0 finite element modeling of an inverse hyperbolic shear deformation theory for the flexural and stability analysis of laminated composite and sandwich plates. Finite Elements in Analysis and Design 2014;80:11–22.

[48] Talha M, Singh B. Static response and free vibration analysis of fgm plates using higher order shear deformation theory. Applied Mathematical Modelling 2010;34(12):3991–4011.

[49] Reddy JN. Mechanics of laminated composite plates and shells: theory and analysis. Second ed.; Boca Raton, USA: CRC press; 2004.

[50] Cottrell J, Hughes T, Reali A. Studies of refinement and continuity in isogeometric structural analysis. Computer methods in applied mechanics and engineering 2007;196(41):4160–83.

[51] Krenk S. Non-linear modeling and analysis of solids and structures. Cambridge, England: Cambridge University Press; 2009.

[52] Srinivas S. A refined analysis of composite laminates. Journal of Sound and Vibration 1973;30(4):495–507.

[53] Grover N, Singh B, Maiti D. Analytical and finite element modeling of laminated composite and sandwich plates: An assessment of a new shear deformation theory for free vibration response. International Journal of Mechanical Sciences 2013;67:89–99.

[54] Kulkarni S, Kapuria S. Free vibration analysis of composite and sandwich plates using an improved discrete kirchhoff quadrilateral element based on third-order zigzag theory. Computational mechanics 2008;42(6):803–24.

[55] Chen J, Dawe D, Wang S. Nonlinear transient analysis of rectangular composite laminated plates. Composite structures 2000;49(2):129–39.

[56] Nosier A, Librescu L, Frederick D. The effects of time-dependent excitation on the oscillatory motion of viscously damped laminated composite flat panels. In: Studies in Applied Mechanics; vol. 24. Elsevier; 1990, p. 249–68.

[57] Khdeir A, Reddy J. Dynamic response of antisymmetric angle-ply laminated plates subjected to arbitrary loading. Journal of Sound and Vibration 1988;126(3):437–45.

[58] Kazancı Z. A review on the response of blast loaded laminated composite plates. Progress in Aerospace Sciences 2016;81:49–59.

[59] Gupta AD, Gregory FH, Bitting RL, Bhattacharya S. Dynamic analysis of an explosively loaded hinged rectangular plate. Computers & structures 1987;26(1-2):339–44.

[60] Adam C, Bouabdallah S, Zarroug M, Maitournam H. Improved numerical integration for locking treatment in isogeometric structural elements, part i: Beams. Computer Methods in Applied Mechanics and Engineering 2014;279:1–28.

[61] Adam C, Bouabdallah S, Zarroug M, Maitournam H. Improved numerical integration for locking treatment in isogeometric structural elements. part ii: Plates and shells. Computer Methods in Applied Mechanics and Engineering 2015;284:106–37.

[62] Prathap G. The finite element method in structural mechanics. Dordrecht, Boston: Kluwer Academic Publishers; 1993.

[63] Hinton E, Campbell J. Local and global smoothing of discontinuous finite element functions using a least squares method. International Journal for Numerical Methods in Engineering 1974;8(3):461–80.

[64] Hassani B, Ganjali A, Tavakkoli M. An isogeometrical approach to error estimation and stress recovery. European Journal of Mechanics-A/Solids 2012;31(1):101–9.

[65] Karama M, Afaq K, Mistou S. A new theory for laminated composite plates. Proceedings of the Institution of Mechanical Engineers, Part L: Journal of Materials: Design and Applications 2009;223(2):53–62.

[66] Rodrigues J, Roque C, Ferreira A, Cinefra M, Carrera E. Radial basis functions-differential quadrature collocation and a unified formulation for bending, vibration and buckling analysis of laminated plates, according to murakami's zig-zag theory. Computers & Structures 2012;90:107–15.

[67] Xiang S, Wang Km, Ai Yt, Sha Yd, Shi H. Analysis of isotropic, sandwich and laminated plates by a meshless method and various shear deformation theories. Composite Structures 2009;91(1):31–7.

[68] Ferreira A, Roque C, Martins P. Analysis of composite plates using higher-order shear deformation theory and a finite point formulation based on the multiquadric radial basis function method. Composites Part B: Engineering 2003;34(7):627–36.

[69] Roque C, Ferreira A, Neves A, Soares CM, Reddy J, Jorge R. Transient analysis of composite and sandwich plates by radial basis functions. Journal of Sandwich Structures & Materials 2011;13(6):681–704.

[70] Pagano N, Hatfield HJ. Elastic behavior of multilayered bidirectional composites. AIAA journal 1972;10(7):931–3.

[71] Pandya B, Kant T. Higher-order shear deformable theories for flexure of sandwich plates—finite element evaluations. International Journal of Solids and Structures 1988;24(12):1267–86.

[72] Wang C, Ang K, Yang L, Watanabe E. Free vibration of skew sandwich plates with laminated facings. Journal of sound and vibration 2000;235(2):317–40.

[73] Chakrabarti A, Sheikh A. Vibration of laminate-faced sandwich plate by a new refined element. Journal

of Aerospace Engineering 2004;17(3):123–34.

## List of Figures

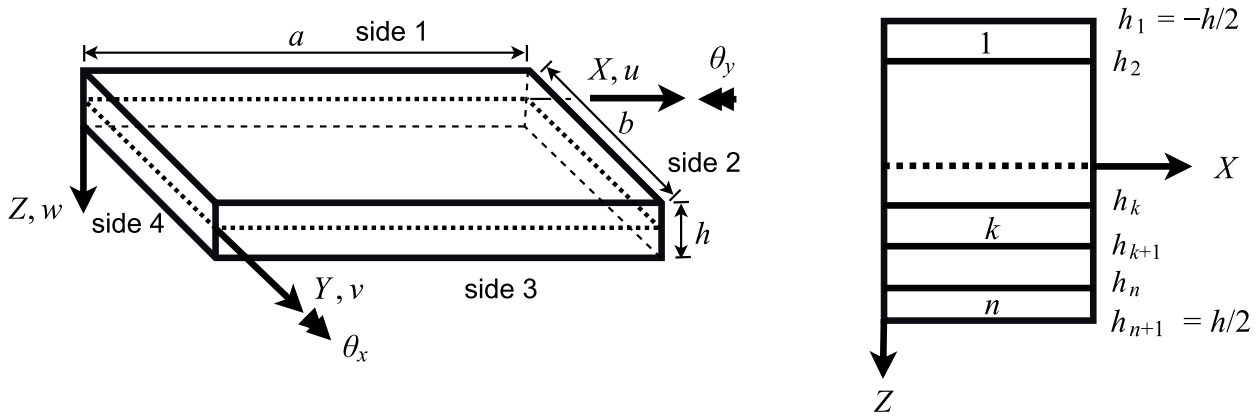


**Fig. 1.** Schematic diagram of a laminated composite plate.

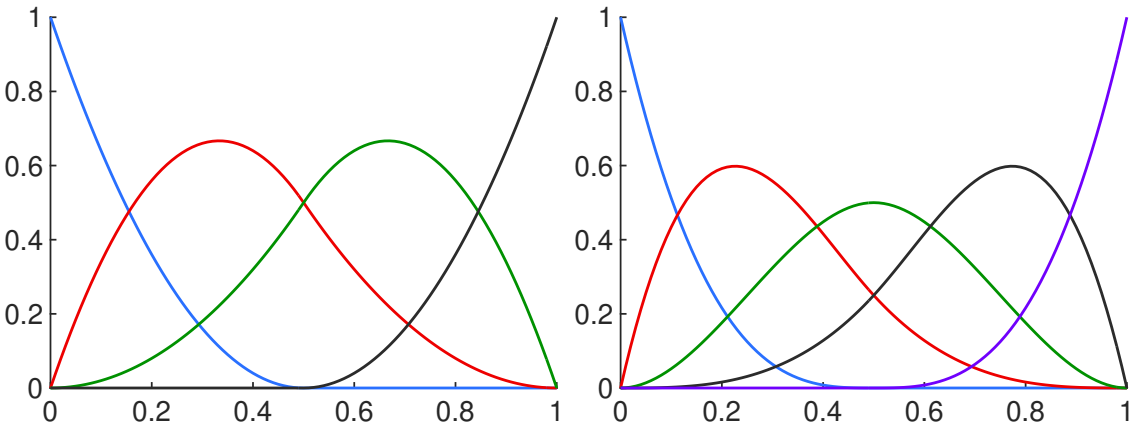


**(a)** $\Xi = \{0, 0, 0, \frac{1}{2}, 1, 1, 1\}$.

**(b)** $\Xi = \{0, 0, 0, 0, \frac{1}{2}, 1, 1, 1, 1\}$.

**(c)** $\Xi = \{0, 0, 0, 0, 0, \frac{1}{2}, 1, 1, 1, 1, 1\}$.

**Fig. 2.** Illustration of $(a)$ Quadratic, $(b)$ Cubic and $(c)$ Quartic B-spline basis functions respectively.

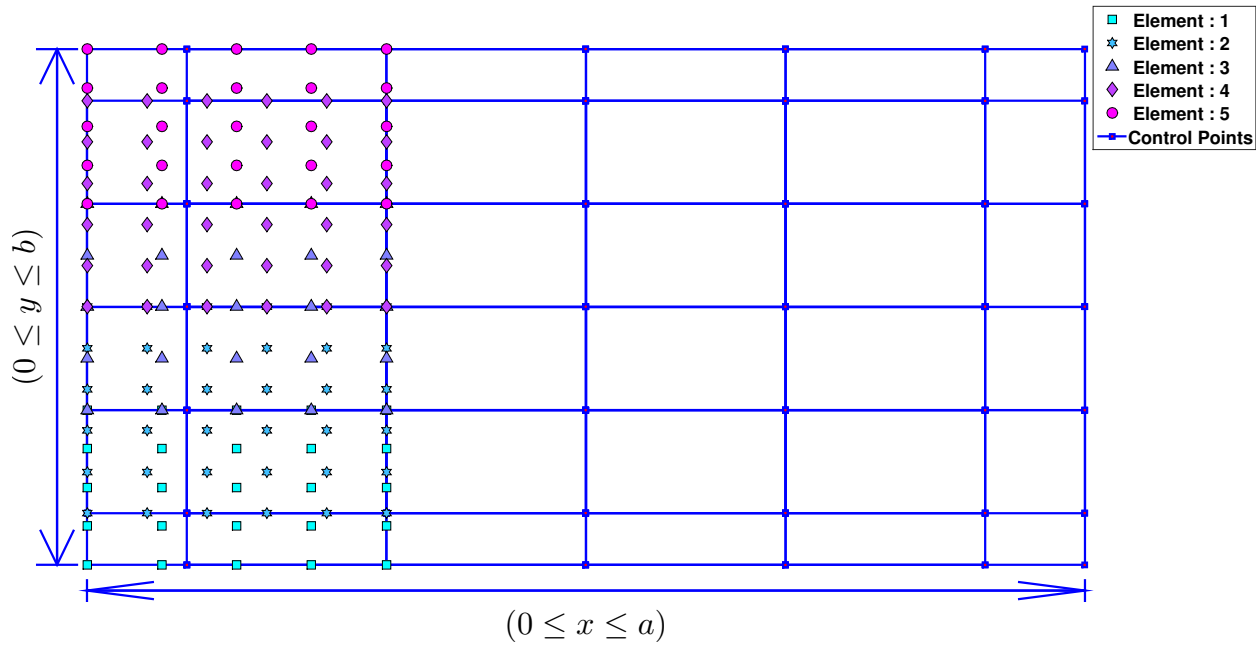


**Fig. 3.** Discretization of rectangular plate using IGA (Control Mesh).

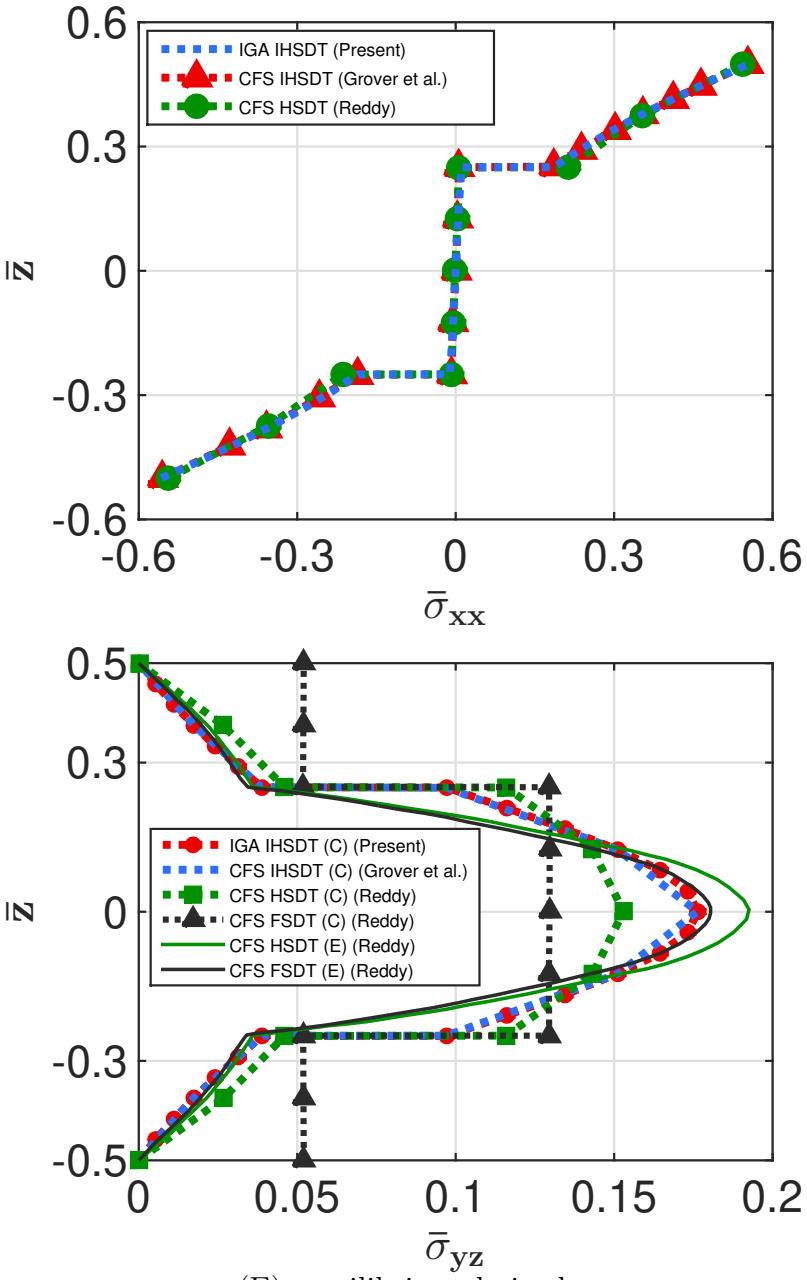


(E): equilibrium-derived
(C): constitutively-derived

**Fig. 4.** Variation of stresses, $\bar{\sigma}_{xx}$ and $\bar{\sigma}_{yz}$ across thickness for $(0^0/90^0/90^0/0^0)$ laminated plate for $a/h = 10$.

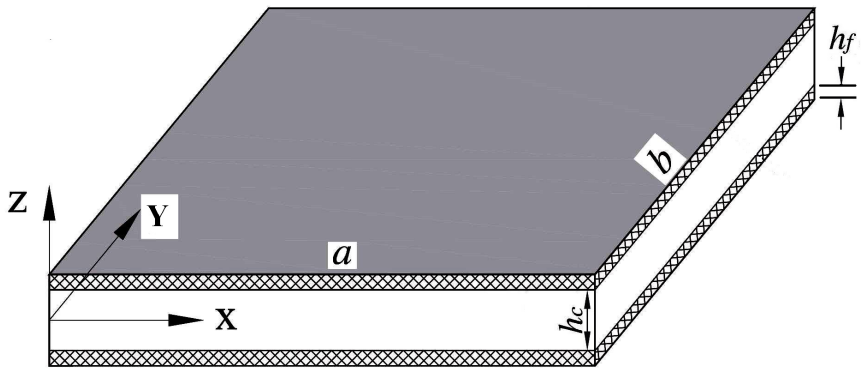


**Fig. 5.** Schematic diagram of a sandwich plate with face sheets and core.

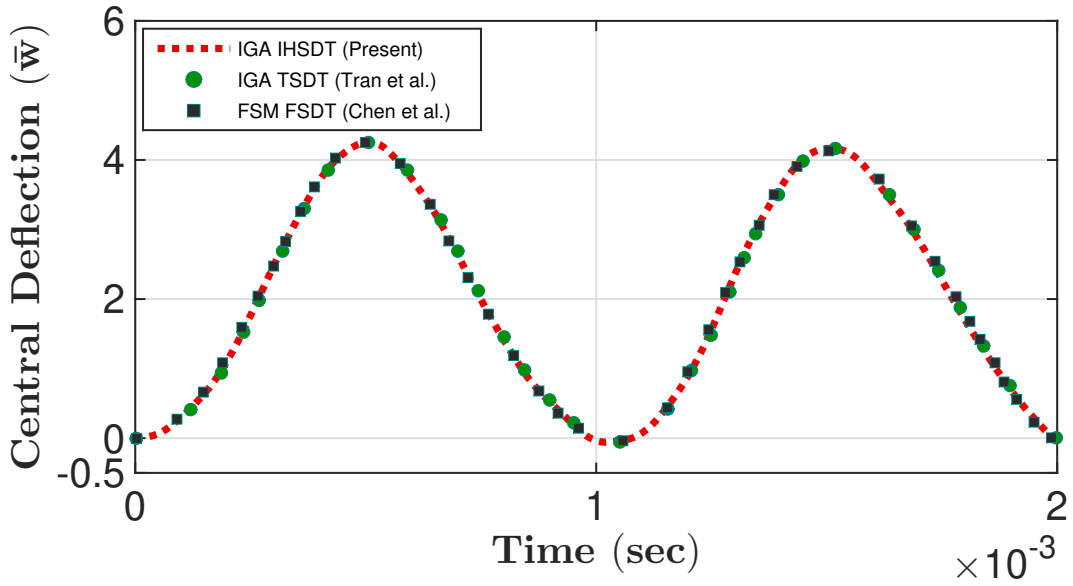


**Fig. 6.** Time history response of the transverse displacement of an orthotropic plate under step loading with spatial uniform distributed load of intensity $1MPa$.

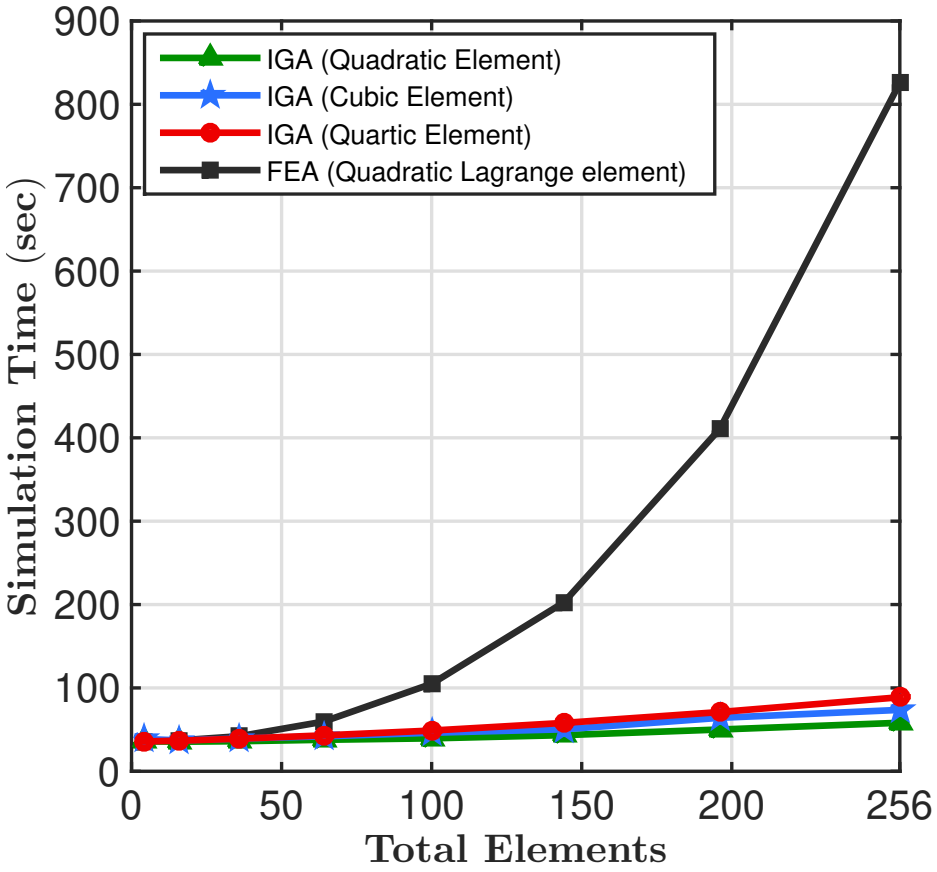


**Fig. 7.** The total simulation time plotted against the total number of elements for an orthotropic plate under step loading with spatial uniform distributed load of intensity $1MPa$ under transient analysis.

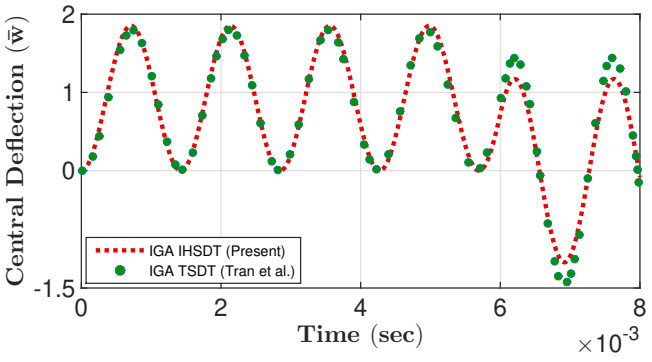


**(a)** Step Loading.

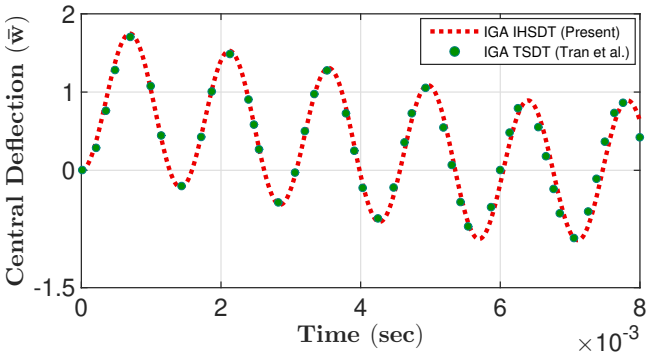


**(b)** Triangular Loading.

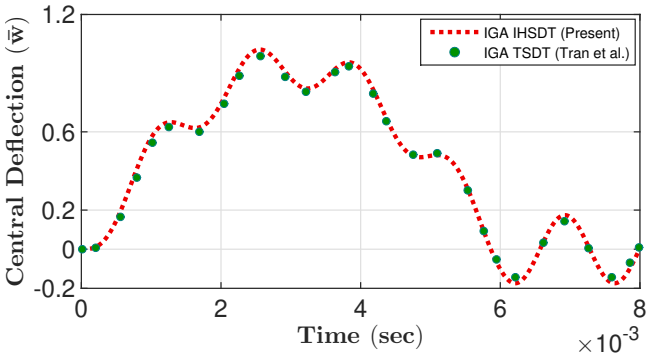


**(c)** Sinusoidal Loading.

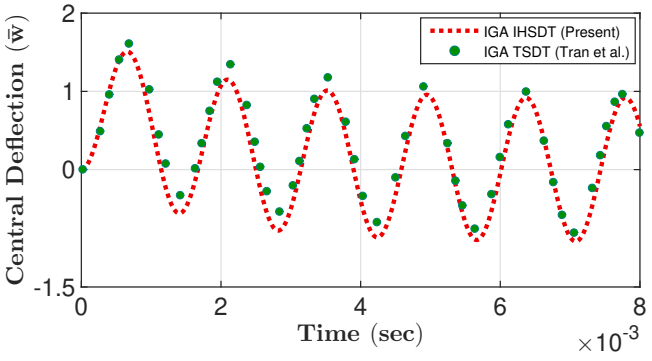


**(d)** Explosive Loading.

**Fig. 8.** Effect of various dynamic loads on the deflection of the cross-ply $(0^0/90^0/0^0)$ square laminated plate.

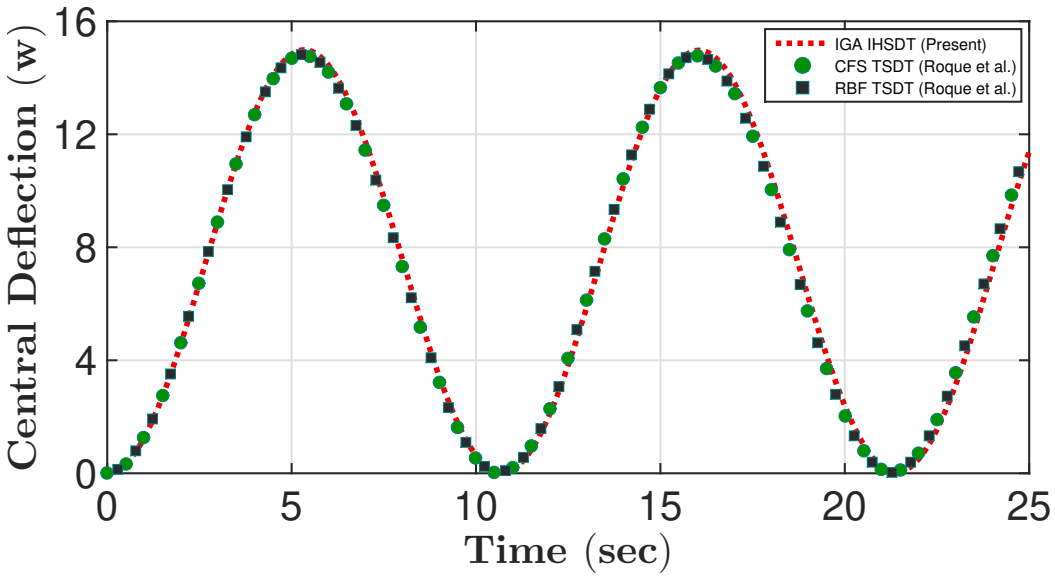


**(a)** Sinusoidal Load Distribution.

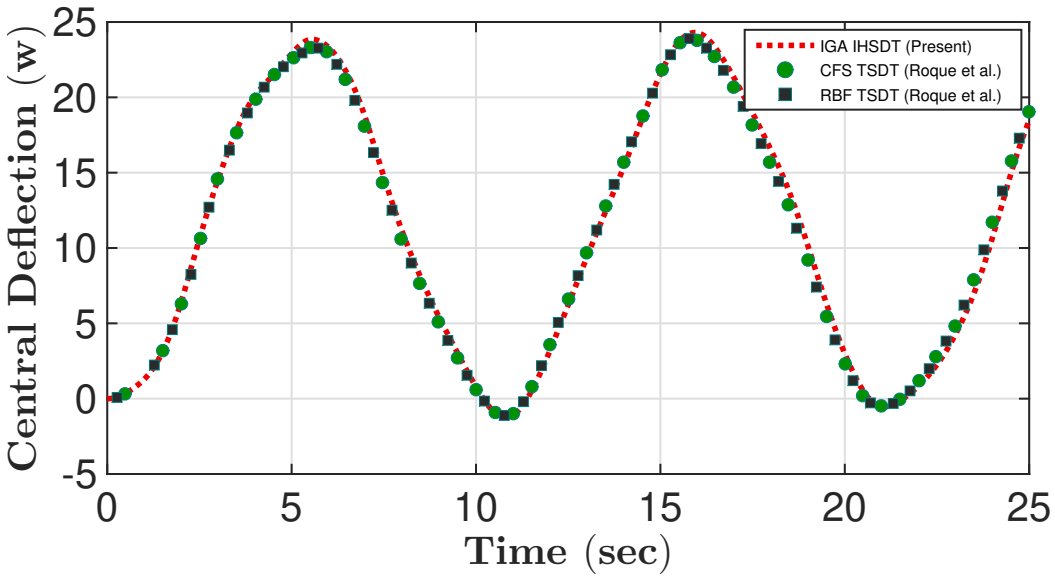


**(b)** Uniform Load Distribution.

**Fig. 9.** Sandwich plate under step loading.

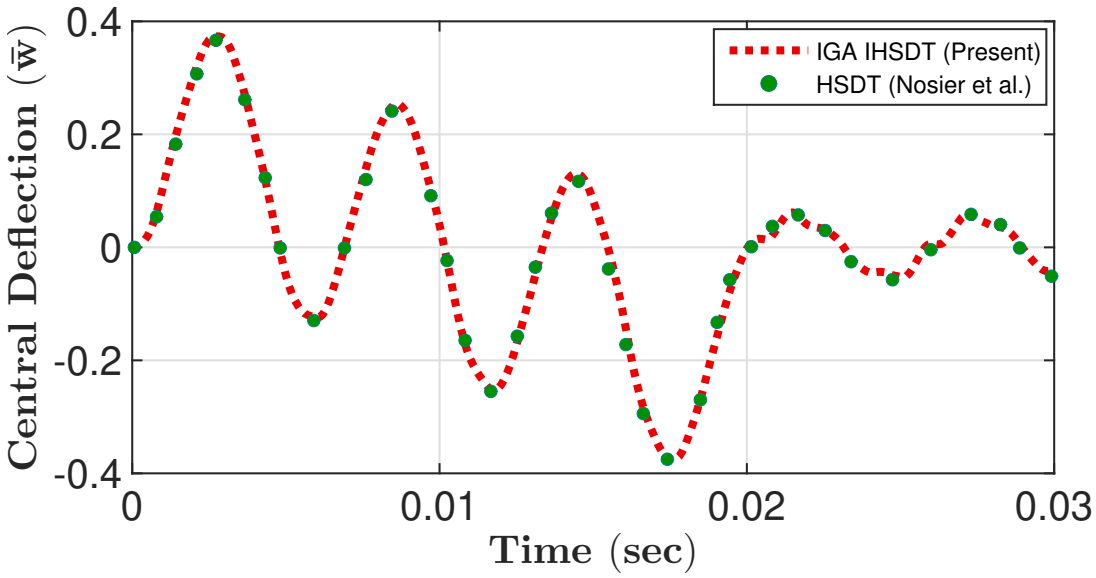


**(a)** r=2 and $t_1 = 0.01sec.$

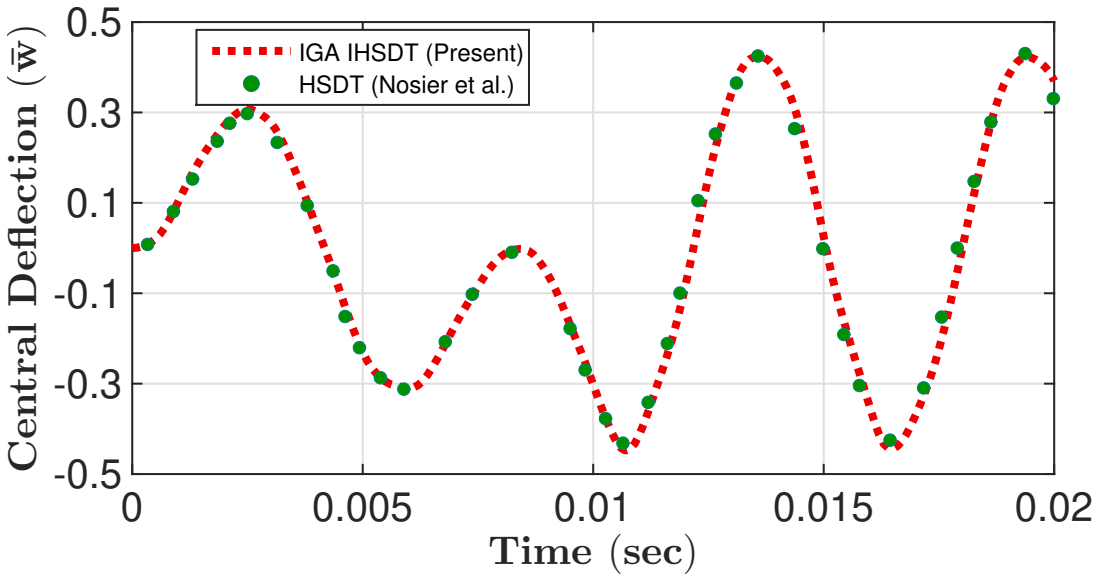


**(b)** r=2.5 and $t_1 = 0.004sec.$

**Fig. 10.** Time-history of the nondimensional central deflection of laminated composite plates to an asymmetric N-shaped pressure pulse.

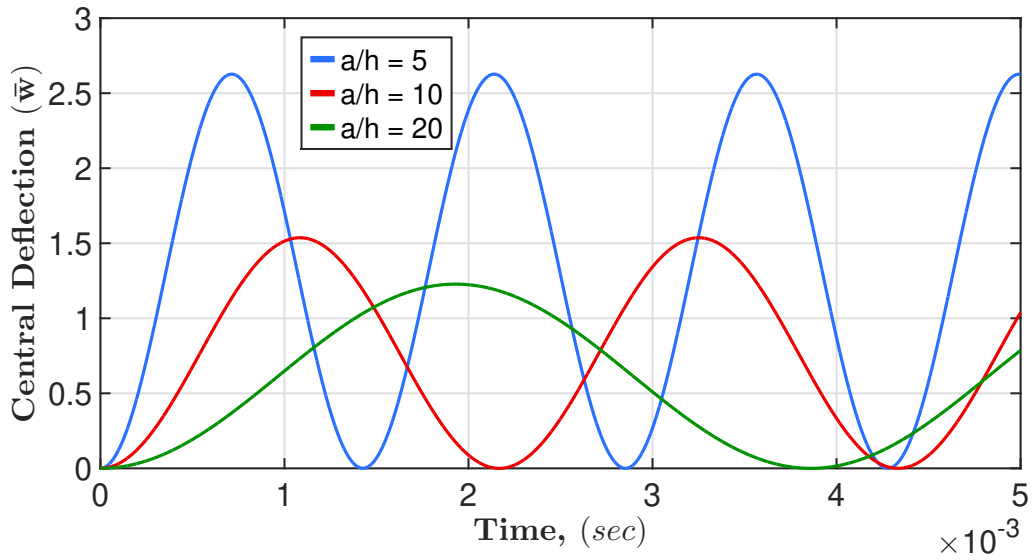


**(a)** Time domain representation.

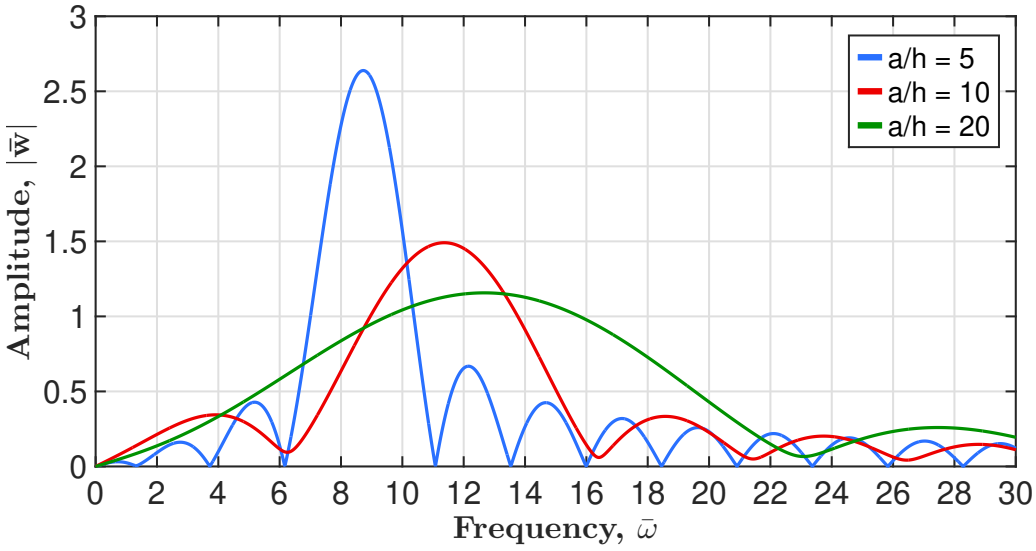


**(b)** Frequency domain representation.

**Fig. 11.** Time-history response and its Fourier transform for the four-layered simply supported symmetric cross-ply square laminated plate under step loading with spatial sinusoidal distributed load.

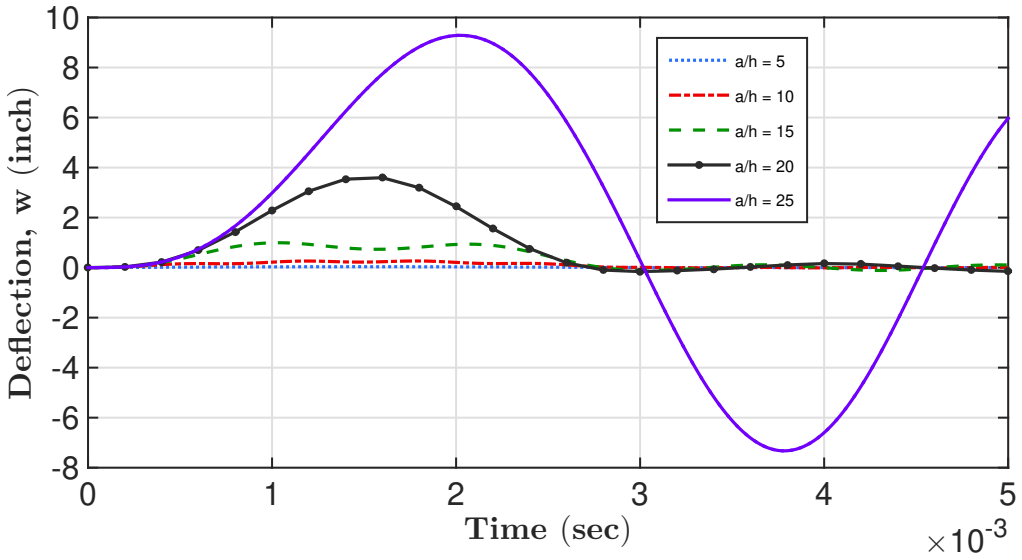


**Fig. 12.** Effect of span-to-thickness ratio on the transient response of cross-ply $(0^0/90^0/90^0/0^0)$ laminated composite plate under sinusoidal loading with spatial sinusoidal distributed load.

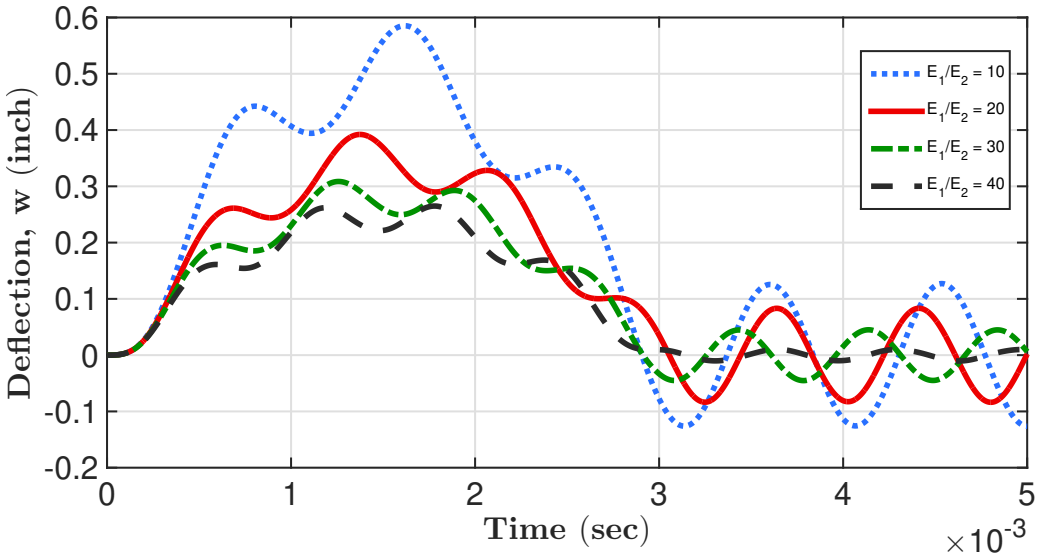


**Fig. 13.** Effect of anisotropy ratio on transient response of cross-ply $(0^0/90^0/90^0/0^0)$ laminated composite plate under sinusoidal loading with spatial sinusoidal distributed load with clamped boundary condition.

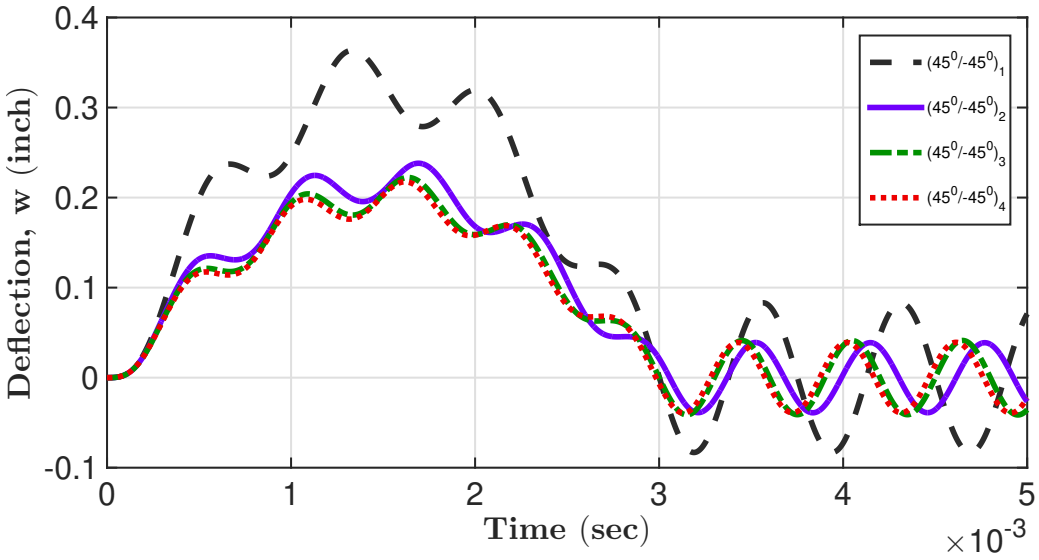


**Fig. 14.** The effect of number of layers on transient response of angle-ply $(45^0/-45^0)_N$ laminated composite plate under sinusoidal loading with spatial sinusoidal distributed load with clamped boundary condition.

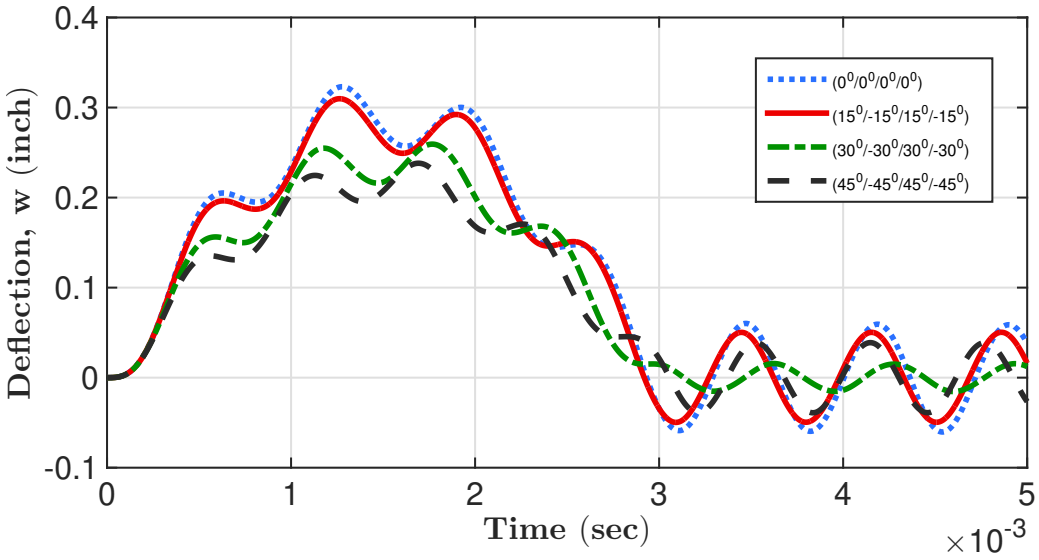


**Fig. 15.** The effect of fiber orientation on the transient response of angle-ply $(\theta/-\theta/\theta/-\theta)$ laminated composite under sinusoidal loading with spatial sinusoidal distributed load with clamped boundary condition.

## List of Tables

**Table 1**
Non-dimensional deflection and stresses for simply supported square laminated $(0^0/90^0/90^0/0^0)$ plate under sinusoidal load.

| $a/h$ | Source / Model | $\bar{w}(\frac{a}{2},\frac{b}{2})$ | $\bar{\sigma}_{xx}(\frac{a}{2},\frac{b}{2},\frac{h}{2})$ | $\bar{\sigma}_{yy}(\frac{a}{2},\frac{b}{2},\frac{h}{4})$ | $\bar{\sigma}_{xy}(0,0,\frac{h}{2})$ | $\bar{\sigma}_{yz}(\frac{a}{2},0,0)$ | $\bar{\sigma}_{xz}(0,\frac{b}{2},0)$ |
|---|---|---|---|---|---|---|---|
| 4 | Pagano [70] | 1.954 | 0.72 | 0.663 | 0.047 | 0.291 | 0.219 |
| | Mantari [11] | 1.921 | 0.74 | 0.635 | 0.048 | 0.269 | 0.254 |
| | Karama [65] | 1.919 | 0.699 | 0.636 | 0.0459 | 0.226 | 0.226 |
| | Reddy [9] | 1.893 | 0.665 | 0.632 | 0.044 | 0.239 | 0.206 |
| | Rodrigues [66] | 1.8931 | 0.6408 | 0.8506 | 0.0436 | - | 0.216 |
| | CFS-IHSDT [46] | 1.9257 | 0.7255 | 0.639 | 0.0473 | 0.27 | 0.25 |
| | IGA-IHSDT (Present) | 1.9257 | 0.7240 | 0.6396 | 0.0473 | 0.2699 | 0.2505 |
| 10 | Pagano [70] | 0.743 | 0.559 | 0.401 | 0.028 | 0.196 | 0.301 |
| | Mantari [11] | 0.73 | 0.561 | 0.395 | 0.028 | 0.176 | 0.3287 |
| | Karama [65] | 0.724 | 0.553 | 0.393 | 0.027 | 0.163 | 0.294 |
| | Reddy [9] | 0.715 | 0.546 | 0.389 | 0.027 | 0.153 | 0.264 |
| | Rodrigues [66] | 0.7227 | 0.546 | 0.4194 | 0.0269 | - | 0.2978 |
| | CFS-IHSDT [46] | 0.7284 | 0.5578 | 0.3947 | 0.0275 | 0.176 | 0.3287 |
| | IGA-IHSDT (Present) | 0.7284 | 0.5572 | 0.3949 | 0.0274 | 0.1763 | 0.3289 |
| 100 | Pagano [70] | 0.439 | 0.539 | 0.276 | 0.022 | 0.141 | 0.337 |
| | Mantari [11] | 0.435 | 0.539 | 0.271 | 0.021 | 0.119 | 0.332 |
| | Karama [65] | 0.435 | 0.538 | 0.27 | 0.021 | 0.118 | 0.324 |
| | Reddy [9] | 0.434 | 0.538 | 0.27 | 0.021 | 0.112 | 0.29 |
| | Rodrigues[66] | 0.4303 | 0.5374 | 0.2704 | 0.0212 | - | 0.3352 |
| | CFS-IHSDT[46] | 0.4345 | 0.5388 | 0.271 | 0.0214 | 0.1271 | 0.3643 |
| | IGA-IHSDT (Present) | 0.4344 | 0.5385 | 0.2710 | 0.0213 | 0.1269 | 0.3643 |

**Table 2**
Static behavior of simply supported sandwich plate ($0^0/C/0^0$) subjected to uniform load.

| $\mathcal{R}$ | Source / Model | $\bar{w}$ | $\bar{\sigma}^1_{xx}$ | $\bar{\sigma}^2_{xx}$ | $\bar{\sigma}^3_{xx}$ | $\bar{\sigma}^1_{yy}$ | $\bar{\sigma}^2_{yy}$ | $\bar{\sigma}^3_{yy}$ |
|---|---|---|---|---|---|---|---|---|
| | Pagano [52] | 258.97 | 60.353 | 46.623 | 9.34 | 38.491 | 30.097 | 6.161 |
| | Pandya and Kant [71] | 258.74 | 62.38 | 46.91 | 9.382 | 38.93 | 30.33 | 6.065 |
| | Touratier [67]† | 253.989 | 60.123 | 47.097 | 9.419 | 38.249 | 30.187 | 6.037 |
| | Karama [67]† | 253.638 | 60.124 | 46.703 | 9.34 | 38.242 | 30.02 | 6.004 |
| 5 | Ferreira et al. [68] | 257.11 | 60.366 | 47.003 | 9.401 | 38.456 | 30.242 | 6.048 |
| | Mantari et al. [11] | 256.706 | 60.525 | 47.061 | 9.412 | 38.452 | 30.177 | 6.035 |
| | FEM-IHSDT [47] | 255.28 | 59.7731 | 46.5043 | 9.3008 | 38.0231 | 29.8858 | 5.9772 |
| | CFS-IHSDT [46] | 255.644 | 60.6752 | 47.055 | 9.4109 | 38.5223 | 30.2056 | 6.0411 |
| | IGA-IHSDT (Present) | 255.623 | 60.55 | 47.033 | 9.4066 | 38.447 | 30.189 | 6.0377 |
| | | | | | | | | |
| | Pagano [52] | 121.72 | 66.787 | 48.299 | 3.232 | 46.424 | 34.955 | 2.494 |
| | Pandya and Kant [71] | 110.43 | 66.62 | 51.97 | 3.465 | 44.92 | 35.41 | 2.361 |
| | Touratier [67]† | 113.964 | 66.544 | 50.679 | 3.378 | 45.431 | 35.278 | 2.351 |
| | Karama [67]† | 114.585 | 66.621 | 49.663 | 3.31 | 45.546 | 34.919 | 2.327 |
| 15 | Ferreira et al. [68] | 114.644 | 66.92 | 50.323 | 3.355 | 45.623 | 35.17 | 2.345 |
| | Mantari et al. [11] | 115.919 | 67.185 | 49.769 | 3.318 | 45.91 | 35.081 | 2.339 |
| | FEM-IHSDT [47] | 115.83 | 66.4816 | 49.1148 | 3.2743 | 45.4806 | 34.6972 | 2.3131 |
| | CFS-IHSDT [46] | 115.82 | 67.2717 | 49.8129 | 3.3209 | 45.9669 | 35.088 | 2.3392 |
| | IGA-IHSDT (Present) | 115.811 | 67.08 | 49.849 | 3.3232 | 45.85 | 35.103 | 2.3402 |

† Xiang et al. [67]

**Table 3**
A non-dimensional natural frequency parameter $\bar{\omega} = (100\omega a)(\rho_c/E_{1f})^{1/2}$ of a $(0^0/90^0/C/90^0/0^0)$ simply supported square sandwich plate with $h_c/h = 0.8$.

| Source / Model | $a/h$ | | |
|---|---|---|---|
| | 6.67 | 10 | 20 |
| 3-Dimensional [54] | 10.5235 | 9.8281 | 7.6882 |
| Wang [72] | 11.414 | 10.555 | 8.029 |
| FEM-TOT [54] | 13.315 | 12.088 | 8.721 |
| CFS-IHSDT [53] | 12.1389 | 11.1572 | 8.3258 |
| IGA-IHSDT (Present) | 12.1395 | 11.1575 | 8.3259 |

**Table 4**
First six natural frequencies of anti-symmetric laminated plate ($0^0/90^0/0^0/90^0$) under simply supported boundary condition with $a/h = 10$.

| Mode | CFS-IHSDT$*$ | IGA-IHSDT (Present) | FEM-IHSDT [53] | 3D [54] | ZZ [54] | ZZ [73] |
|---|---|---|---|---|---|---|
| 1 | 14.8390 | 14.8390 | 14.8302 | 14.7668 | 14.754 | 14.712 |
| 2 | 33.1887 | 33.1901 | 33.1266 | 32.7998 | 32.772 | 32.178 |
| 3 | 33.1887 | 33.1901 | 33.1266 | 32.7998 | 32.772 | 32.178 |
| 4 | 44.7320 | 44.7341 | 44.6260 | 44.1645 | 44.011 | 42.651 |
| 5 | 55.6689 | 55.6916 | 55.4164 | 54.5818 | 54.571 | 51.827 |
| 6 | 55.6689 | 55.6916 | 55.4164 | 54.818 | 54.571 | 51.827 |

$*$ Results obtained using method prescribed in the literature [53]

**Table 5**
A non-dimensional natural frequency parameter $\bar{\omega} = (\omega a^2/h)(\rho/E_2)^{1/2}$ of a $(0^0/90^0/90^0/0^0)$ simply supported laminated square plate for various $a/h$ using step loading.

| Source / Model | $a/h$ | | |
|---|---|---|---|
| | 5 | 10 | 20 |
| 3-Dimensional† [54] | 8.5611 | 11.2981 | 12.721 |
| CFS-TOT† [54] | 8.7167 | 11.424 | 12.771 |
| CFS-SDTSF† [46] | 8.7170 | 11.4243 | 12.7711 |
| CFS-ITSDT† [46] | 8.6241 | 11.3507 | 12.7424 |
| CFS-IHSDT† [46] | 8.6216 | 11.3481 | 12.7413 |
| IGA-IHSDT† (Present) | 8.62155 | 11.348 | 12.7413 |
| FFT (Present)∗ | 8.694 | 11.340 | 12.740 |

† Eigenvalue
∗ Fast Fourier Transform (FFT)